REACTION KINETICS OF Pd AND Ti-Al FILMS ON Si

Thesis by

Robert William Bower

In Partial Fulfillment of the Requirements

For the Degree of

Doctor of Philosophy

California Institute of Technology

Pasadena, California

1973

(Submitted April 30, 1973)

To my wife, Willa

who sacrificed without hesitation ...

who encouraged without limit.

ACKNOWLEDGMENTS

I am especially indebted to Dr. J. W. Mayer for the encouragement he provided me to return to graduate school and to Dr. Mayer and Dr. M. A. Nicolet for their guidance and assistance in this work.

The collaboration with Dr. Dag Sigurd and Dr. R. E. Scott was most rewarding and enjoyable. For help and guidance in using the 3 MV accelerator I am especially indebted to Dr. C. A. Barnes and the members of the Kellogg Laboratory staff. For guidance in the X-ray diffraction analysis I am indebted to Dr. Pol Duwez. Discussions with Dr. Carver Mead and Dr. James McCaldin provided me with a great deal of help in the course of this work. The aid of Mr. J. Devaney with the scanning electron microscopy and Mr. W. Hewett on the electron microprobe was invaluable.

Stimulating discussions with the staff of the TRW Systems Microelectronics Laboratory, and especially Mr. J. Buie, Mr. R. Miller, Mr. L. Braun and Dr. M. Bloom; and use of the facilities of this laboratory were extremely helpful to me in completing this work. Finally my thanks to Ms. K. Current and Ms. C. Philips who prepared this manuscript with unparalleled speed and many helpful suggestions.

Financial assistance from Air Force Cambridge Research Laboratories (Graduate Research Assistantship) and the Corning Glass Foundation (Corning Glass Fellowship) is gratefully acknowledged. The Caltech 3 MV accelerator was supported by the Office of Naval Research and the National Science Foundation.

ABSTRACT

The growth of compound phases from thin film layers of Pd and Ti-Al deposited on Si is described in this work. The growth kinetics and composition of the compound phases were measured utilizing 2 MeV ^4He backscattering. Crystalline structure and film texture effects of the compounds layers were measured by X-ray diffraction techniques.

The Pd-Si system was first studied by depositing 1000 to 3000Å of Pd onto a Si substrate and heating to 200 to 700°C. A single phase of material with a composition Pd_2Si developed when specimens were heated to a temperature of 200°C. The phase grows at a rate proportional to $(time)^{\frac{1}{2}}$ indicating transport limited growth. The temperature dependence of the growth constant was found to be expressible as a single activation energy of approximately 1.50 eV over the 200 to 275°C temperature range where growth kinetics were measured.

The X-ray diffraction data indicated that the Pd_2Si phase which formed has the crystalline structure of Pd_2Si known from metallurgical studies of bulk materials. The Pd_2Si layers which formed from the thin film structures were found to be oriented with the hexagonal basal plane parallel to the substrate material. The degree of the preferred orientation of the Pd_2Si depends on the Si substrate orientation. By far the highest degree of orientation was found when the Pd_2Si was formed on <111> -Si.

The more complex Si-Ti-Al system is treated following the Pd-Si system. In this case a layer of Ti and then Al was evaporated on Si after which the specimens were heated to temperatures of 400° to 500°C.

Backscattering of ^4He ions was used to measure growth kinetics and composition of compound phases which develop. While the spectra are more complex the same basic analysis techniques developed for the Pd-Si system were applicable. While no measurable reaction of the Si and Ti was found in this temperature range, the Ti-Al reacts to form a phase of $TiAl_3$. The rate of formation of $TiAl_3$ was also found to be proportional to $(time)^{\frac{1}{2}}$ indicating transport limited growth. The temperature dependence of the growth constant was found to be again expressible by a single activation energy over the temperature range measured. The value of activation energy was found to be approximately 1.85 eV.

The X-ray diffraction analysis indicates that a single phase of $TiAl_3$ forms until the entire Ti layer is consumed. At this point Si reacts with the system displacing most of the Al to form a Si-rich Ti-Al-Si ternary phase.

The Ti-Al metal system is used to make contact to Si in integrated circuit applications. The $TiAl_3$ and subsequent Si-rich Ti-Al-Si ternary formation in this system can be directly related to severe erosion of metal -Si contact areas which result in failure of the integrated circuits.

The measured rate of formation of $TiAl_3$ found from the backscattering measurements allows the thickness of Ti to be chosen large enough so that heat treatments following metal deposition will not cause contact failure. Thus, the rate kinetics of $TiAl_3$ formation measured by 2 MeV ^4He backscattering is found to have practical application in predicting and controlling a failure mechanism in an integrated circuit metallization scheme.

TABLE OF CONTENTS

CHAPTER I

INTRODUCTION

It is common practice in the semiconductor industry to deposit one or more layers of metal 1000 to 10,000Å thick on the surface of integrated circuit structures to form conductive contact to selected areas of Si.[1] To form good electrical contact between the metal and Si regions it has usually been found necessary to heat the structure to between 400 and 500°C after the metal has been deposited.[1] At the time this investigation began in January 1971, heat treatments of 400 to 500° were known to be sufficient to cause certain metal silicides to form.[2-4] However, little was known of the structure of these substances and there were no data available on the rate kinetics of their formation.

This work is an investigation of the kinetics of growth, composition and structure of silicide and aluminide phases which form when thin layers of Pd and Ti-Al are deposited on Si and subsequently heated to temperatures of 200 and 600°C. Palladium silicide is useful as a contact material for various Si device applications.[5-8] However, in this work, Pd-Si is primarily presented to illustrate a simple system to develop the backscattering analysis techniques used to detect and measure the growth kinetics and composition of compound phases. Compound formation in the more complex Si-Ti-Al system is then studied and found to provide the key to understanding a failure mechanism in the Ti-Al metallization system used to form contacts in Si integrated circuits.

Numerous intermetallic and silicide phases have been identified for metal systems commonly used in thin film applications.[9,10] Metal

silicide phases are shown in figure 1 which is reprinted from Goldschmidt.[9] This figure illustrates that many metals have numerous silicide phases. Similar phase diagrams are also known for many metal-metal systems.[10] The phases identified in these diagrams represent equilibrium conditions, however. Generally the compounds shown were produced by slowly cooling a liquid phase mixture of the metal and silicon. In contrast, the silicides formed from thin film couples heated to temperatures below 600°C must depend on solid state transport for mixing of the metal and silicon. This process is generally far from equilibrium; dominated almost entirely by kinetics. Equilibrium diagrams provide excellent clues to possible compounds that may develop when a thin film couple reacts at low temperature; however, these diagrams are not sufficient to describe which phases will result from the kinetic processes which occur when these thin films are heated. One phase may dominate because it is more efficient in transporting the material flux needed to continue the mixing process.[11] Alternatively, a phase may be absent because it does not nucleate at the low temperatures involved. Finally, phases which form in the kinetic mode may not have a direct equilibrium counterpart. Such a case is described in this work for the Ti-Al-Si system where the ternary found differs significantly from its equilibrium counterpart. Non-equilibrium phases have also been identified in the study of amorphous materials.[12]

Backscattering of MeV ^{4}He ions provides a unique tool to investigate compositional changes in thin film structures used in the Si integrated circuit technology. Compositional changes of a few percent can readily be detected and the depth scale provided by energy loss typically allows a thickness resolution about 100Å.[13] A 2 MeV ^{4}He beam may be used to measure metal films ranging up to 3000 to 10,000Å in thickness.

Fig. 1 This chart was adapted from figures in "Interstitial Alloys," by H. J. Goldschmidt, Plenum Press 1967. The metal-silicon phase diagrams are arranged in a pattern representing the position of the metal in the periodic table. The metal-silicide phases are highlighted in these diagrams.

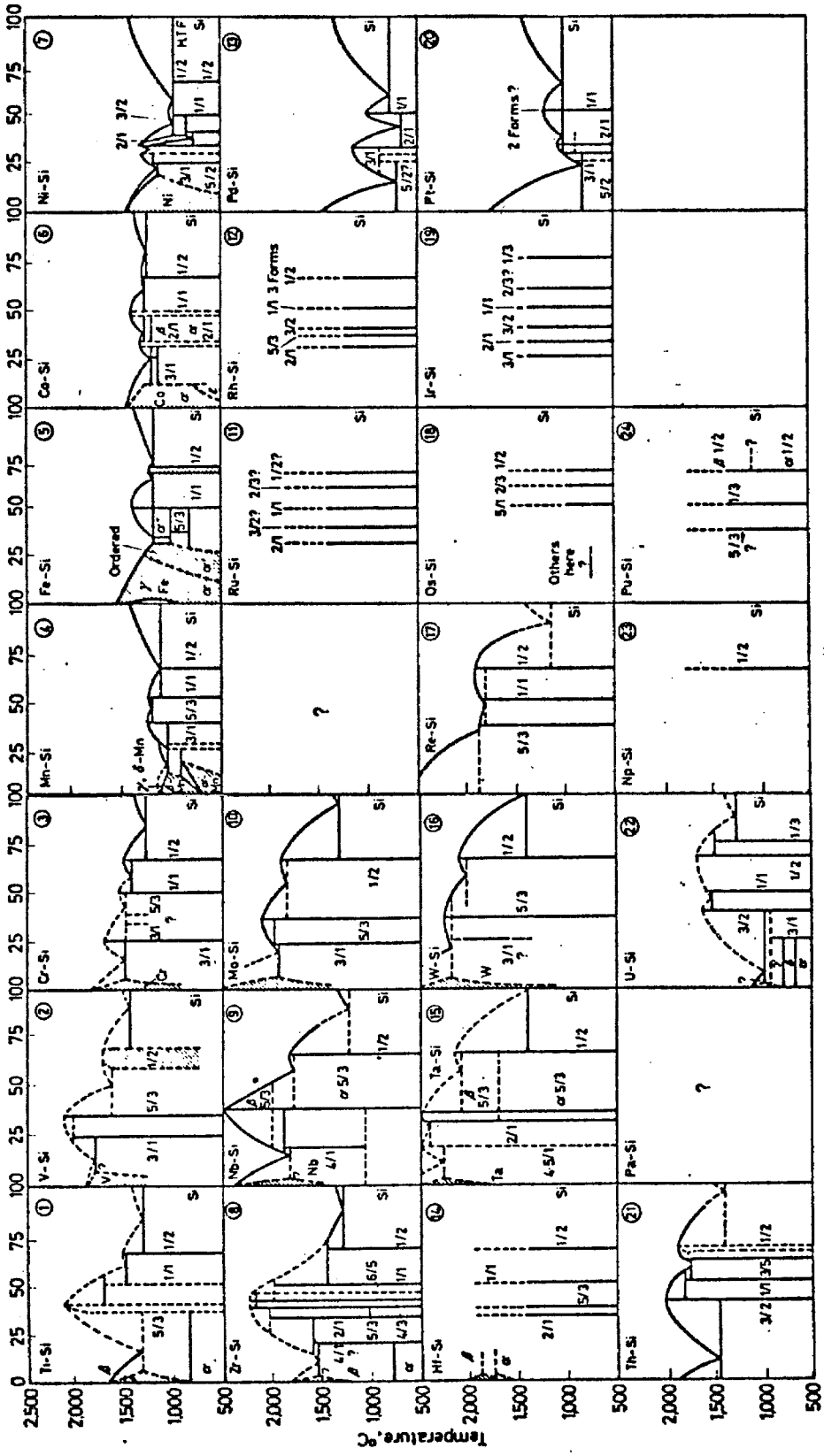
SILICIDES
At per cent silicon
Temperature, °C
Ti-Si
V-Si
Cr-Si
Mn-Si
Fe-Si
Co-Si
Ni-Si
Zr-Si
Nb-Si
Mo-Si
Ru-Si
Rh-Si
Pd-Si
Hf-Si
Ta-Si
W-Si
Re-Si
Os-Si
Ir-Si
Pt-Si
Th-Si
Pa-Si
U-Si
Np-Si
Pu-Si
Ordered
2 Forms?
Others Here ?

Fig. 1

In this work, backscattering techniques were used to detect the development of silicide and intermetallic substances in the range of a few hundred to a few thousand angstroms in thickness.

The work reported here developed from an observation in late 1970 that distinct compositional changes were detectable in the backscattering spectra of thin film layers of Pt deposited on Si that had been heated to 450°C for 30 minutes.[14] The present study began in early 1971 to determine if the compound formation observed in the Pt-Si case was part of more general phenomena. The systems studied included Pd-Si, Ti-Si, Cr-Si, and Mo-Si. All of these couples developed compositional steps in their backscattering spectra after heat treatments of less than 600°C except Mo-Si which required 900°C for a step to develop.[15] In the case of Pd-Si, Cr-Si and to a lesser extent Ti-Si the compositional changes were so distinct that the silicide region could be directly measured to determine the rate kinetics of the silicide growth process.[15] The Pd-Si and Cr-Si spectra indicated that the silicide films were uniform to within approximately 100Å over the one mm spot diameter of the analyzing beam. These were the first reported rate kinetics for silicide films. Many other systems were subsequently measured and found to form approximately stochiometric compounds from couples of Pd-Al, Hf-Si, Ti-Al and more complex substances such as Si-Pd-Cr and Si-Ti-Al.[16,17,18,19] All of these systems formed compound regions of approximately 1000Å in thickness after heating to 200 to 600°C for tens of minutes. In all cases except Pt-Si and Hf-Si only one detectable compound phase developed. In the cases of Pt-Si and Hf-Si two phases were found.[17,20] These studies indicate that compound formation was the

rule rather than the exception at low temperatures.

In most cases where kinetics were measured, the rate of growth was proportional to the square root of time indicating that material transport across the film limited the process.[15,17,19,20] Thus, the reaction kinetics associated with interfaces or silicide formation does not appear to limit the process in general. In the cases of the Cr-Si and Mo-Si where single phases of $CrSi_2$ and $MoSi_2$ were found to form at a rate linear in time, it is possible that an oxide interface between the Si and metal may limit the process rather than the compound formation itself.[15] Activation energies found for the cases studied ranged from 1.5 to 2. eV. This range of activation energy may be compared with the 1 eV activation energy of interstitial diffusion of carbon in ferrite and the 2.3 eV activation energy of typical substitutional diffusion in metals.[9] The silicides and aluminides which have been studies are classified as near interstitial alloys and might be expected to have activations energies for transport which range between the interstitial case of carbon diffusion in metal and that of substitutional diffusion in metals.[9] The rate constant for the systems studied was typically 10^{-13} cm^2/sec in the range of temperature measured. This corresponds to 1000Å of growth in 1000 seconds. The same rate constant would require 4 months to grow a layer 10 micrometers thick. Thus, it is not surprising that so little work was done on kinetics of compound formation in these films, since the thicknesses involved lie outside the range of most measurement techniques.

Backscattering techniques were used to measure the kinetics and composition of the compound formation in the system studied in

this work. This technique does not provide the structural information needed to identify compound phases, however. In order to identify structural phases x-ray diffraction techniques were used to complement the backscattering data. Powder diffraction and diffractometer measurements were used to identify the compound phases formed, while pole figure analysis was used to study orientation effects in the Pd_2Si films.

The chemical composition of large area Al-Ti on Si samples were measured with an electron microprobe. This was required to measure the Ti-Al-Si ternary which forms since backscattering did not conveniently allow the relative amount of Si and Al to be determined. The patterned contact pattern samples used to study the properties of the Al-Ti metallization of Si were analyzed with the electron microprobe and both optical and scanning electron microscopy. All three of these tools provided an areal resolution of one micron or better required to determine structural changes in the contact area. The 1mm diameter ^4He backscattering beam was not useful to study the small contact window areas used in this part of the investigation.

The experimental techniques and sample preparation used in this work is described in Chapter II.

Chapters III and IV are devoted to a study of two practical thin film systems used in the semiconductor industry. In Chapter III, the composition, rate kinetics and crystalline structure of Pd_2Si formed from deposited layers of Pd on Si heated to 200 to 700°C is presented. In this case, the backscattering energy spectrum is quite straightforward and is used to develop the analysis techniques required

to detect, measure rate of growth and composition of compound phases which develop in these thin films. X-ray analysis of the Pd-Si was used to identify Pd_2Si and also to determine film texture effects of this material which depend on the Si substrate orientation. This example is used to illustrate that uniform, highly oriented single phase layers can result from low temperature compound formation in thin films.

The composition, rate kinetics and crystalline structure of $TiAl_3$ is described in Chapter IV. The $TiAl_3$ forms by heating a thin film system consisting of a Ti layer deposited on a Si substrate and an Al layer evaporated on top of the Ti. The backscattered energy spectrum which results in the Si-Ti-Al are more complex than for Pd-Si; however, the same basic analysis techniques developed in the Pd-Si case may again be used. The x-ray analysis reveals that $TiAl_3$ first forms when the Si-Ti-Al is heated in the range of 400 to 500°C, however, after all the Ti is consumed the x-ray analysis indicates that a silicon rich Ti-Al-Si ternary is formed. Prior to the reaction of all the Ti in the $TiAl_3$ formation, the Si has neither reacted with the Ti or diffused through the Ti into the Al.

Chapter V describes the Si-Ti-Al metal system used to form contacts and interconnections to Si in the semiconductor industry.[21,22] This metal system provides a way to avoid the Si pits formed in contact areas when an Al metallization is used. The Si-Ti-Al system fails, however, when the heating process extends beyond certain critical times and temperatures. This failure process is found to directly relate to the formation of $TiAl_3$ and subsequent formation of the Si

rich Ti-Si-Al ternary. Thus, the kinetics of $TiAl_3$ formation provides the key to understanding and predicting a failure mechanism in a Si-Ti-Al metallization system used in the semiconductor industry.

Publications Associated with This Work

1. R. W. Bower and J. W. Mayer, Appl. Phys Lett. 20, 359 (1972). "Growth Kinetics Observed in the Formation of Metal Silicides on Silicon."
2. R. W. Bower, Submitted, Appl. Phys. Lett. "Characteristics of Aluminum-Titanium Contacts on Silicon."
3. R. W. Bower, Submitted, J. Appl. Phys. "Low Temperature Intermetallic Phase Formation on Evaporated Ti and Al Layers on Si."
4. R. W. Bower, Submitted, Solid-State Elec. "Failure Mechanism in Ti-Al Contacts to Si."
5. R. W. Bower, D. Sigurd and R. E. Scott, Submitted, Solid-State Elec. "Formation Kinetics and Structure of Pd_2Si Film on Si."

CHAPTER II

EXPERIMENTAL TECHNIQUES AND SAMPLE PREPARATION

The primary tool used in this investigation was 2 MeV ^{4}He backscattering. The kinetics of growth and composition of compound phases was measured using the backscattering technique. Crystal structure, chemical composition and Si contact hole erosion required other tools for measurement; x-ray diffraction was used to study crystal structure and the electron microprobe was used to determine chemical composition in cases where the atomic species could not be determined from backscattering. Both optical and scanning electron microscopy were used to study Si contact hole erosion.

All of the experimental techniques used in this investigation have been described elsewhere, however, a brief description of them will be included here.

A. Backscattering Analysis

The backscattering analysis was carried out on the 3 MeV Kellogg machine utilizing a solid state nuclear particle detector positioned at a scattering angle $\theta = 180° - \theta'$, where $\theta' = 10°$. A schematic diagram of the backscattering chamber and electronics is shown in figure 2. The samples measured for kinetics and composition of compound formation were mounted on a multiple target holder where they were sequentially rotated into normal incidence with the incoming beam. The channeling measurements described in the Appendix utilized a two-axis goneometer described elsewhere.[23] A beam spot of approximately

Fig. 2 This figure illustrates the experimental arrangement used to measure the backscattering spectra of the thin film structures in this investigation. The incoming beam strikes the sample at normal incidence and the ^{4}He particles scattered into an angle θ' are analyzed with a solid state nuclear particle detector. The output of the detector is amplified and stored in a pulse height analyzer. A simple multitarget holder was used instead of the 2-axis goniometer shown in this figure for the kinetics and composition measurements. The goniometer was used in the channeling measurements.

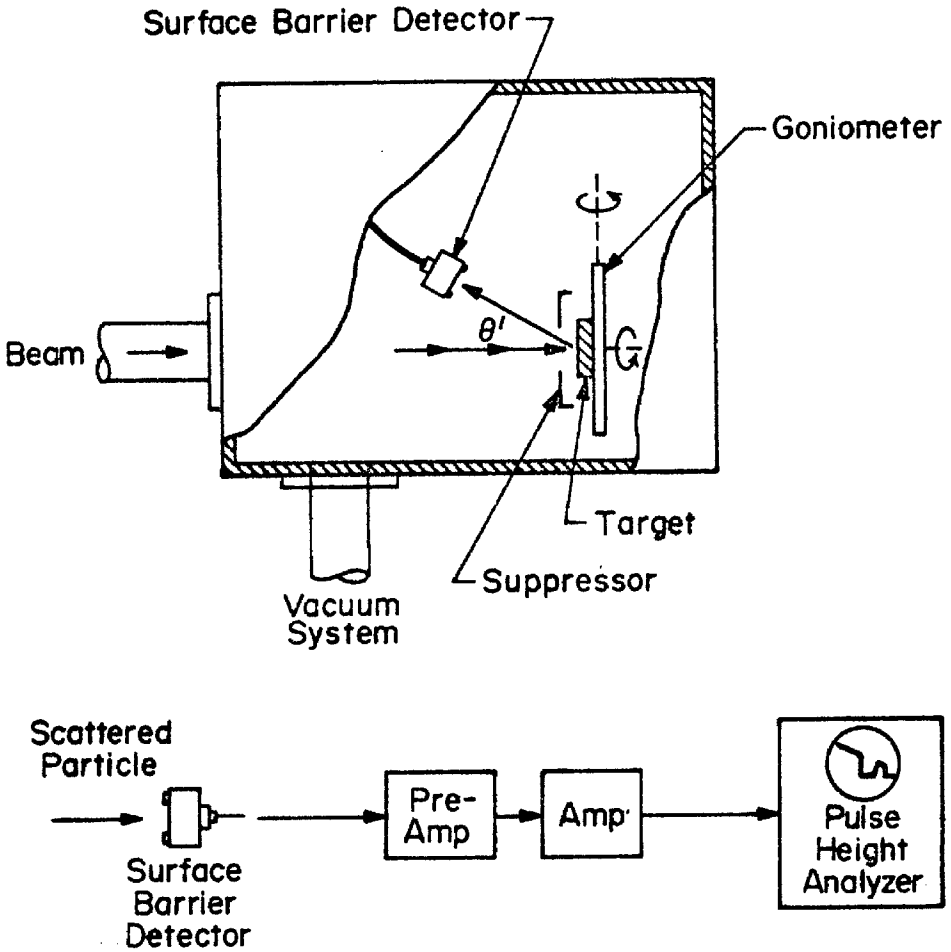
Surface Barrier Detector
Goniometer
Beam
θ'
Target
Suppressor
Vacuum System
Scattered Particle
Surface Barrier Detector
Pre-Amp
Amp
Pulse Height Analyzer

Figure 2

$1mm^2$ was used to study the samples in this investigation.

B. X-Ray Diffraction Analysis

Structural identification of Pd_2Si, $TiAl_3$ and the Ti-Al-Si ternary were performed using a standard Debye-Scherrer powder diffraction camera. Diffractometer analysis supplemented this technique and proved useful in identifying $TiAl_3$.

Pole figure analysis was used to identify orientation effects in the Pd_2Si films. In this case a three-axis goneometer was mounted on a standard diffractometer. A description of the experimental technique involved in pole figure analysis is described in the literature.[24] All of the x-ray diffraction measurements were made with CuKα radiation.

C. Electron Microprobe and Scanning Electron and Optical Microscopy

A great deal of the compositional analysis of the Si-Ti-Al system could not be accomplished by 2 MeV ^4He backscattering. This resulted from the overlap in energy of the Al and Si spectra which prevented compositional analysis of these two species. In addition, the Si contact hole analysis required better than one micron resolution of the topology of the substrate surface.

The use of the electron microprobe provided a solution to the problem of compositional analysis of the Ti-Al-Si ternary on both large area and patterned contact samples. The electron microprobe used employs a nondispersive crystal monochrometer detection system which easily resolved the characteristic x-rays from Si and Al. The

surface topology was analyzed using a high magnification optical microscope and a scanning electron microscope (SEM). The SEM was fitted with a two axis goneometer. This allowed the cleaved edges to be viewed at their optimum angle.

D. Sample Preparation

1. Pd-Si

Samples were prepared by depositing 1000 to 3000Å of Pd onto large area silicon substrates at temperatures ranging from 25 to 100°C. Electron beam and filament evaporation were used. Both p and n type silicon was used with <111>, <110> and <100> orientations. In addition, Pd was evaporated onto amorphous Si layers which were formed by either vacuum evaporation of Si at 100°C or an ion implantation of 5×10^{15} Si ions/cm^2 at 50 keV and a substrate temperature of 25°C.[25] The Si surfaces were cleaned in hot HNO_3 and H_2SO_4, followed by a HF etch and H_2O rinse just prior to evacuation. In certain specified cases an oxide interface was purposely created by boiling the Si in H_2O just prior to pump down.

Heat treatments were performed in a vacuum anneal furnace at a pressure of 2 to 8×10^{-5} Torr. The heat treatments were essentially isothermal. The anneal times were chosen to be appreciably longer than the measured heating and cooling periods (<40 seconds).

The powder diffraction samples were prepared by chemically etching the Si substrate in an Ethylene-diamine-Pyrocatethol etch and pulverizing the remaining Palladium Silicide film.[26] The particles of the silicide were then attached to a .2mm glass rod with an adhesive binder. The resulting powder sample was not randomly oriented as

desired but favored planes parallel to the original substrate surface.

2. Si-Ti-Al

The thin films of Al-Ti and Al were electron beam evaporated in a chamber evacuated to 10^{-7} torr onto a Si substrate which was heated to a temperature of 100 C. The Ti was first evaporated onto the substrate and Al followed during a single evacuation of the vacuum chamber. In some cases the films were evaporated onto an oxidized wafer. The backscattering samples typically consisted of a 1200Å layer of Ti covered with 10,000 to 17,000Å of Al, while the x-ray samples were prepared with 1500 to 3000Å of Ti covered with 20,000 to 30,000Å of Al. The samples were heated in a N_2 atmosphere in a three zone furnace accurate to $\pm$ 2°C.

In some cases the unreacted Al was removed from the surface after heat treatment in a selective etch of 40 parts H_2PO_3, 9 parts HNO_3 and 4 parts H_2O. This etchant removes Al at a rate of approximately 1000Å per minute while etching less than 50Å per minute of $TiAl_3$. X-ray powder samples of $TiAl_3$ and the Ti-Al-Si tenary were formed by chemically etching the excess Al from the surface where it was then loaded into a .2mm capillary tube. This removal technique was only successful on samples where the metal was deposited on Si and all the Ti was reacted. The resulting $TiAl_3$ sample was contaminated with some of the ternary. The ternary powder sample was produced by continuing to heat the material for a short period of time after all the Ti was consumed in the $TiAl_3$ formation.

3. Si Contact Patterns

The thin films of Al-Ti and Al used for contact metalization

were electron beam evaporated in a chamber evacuated to 10^{-7} torr onto a <100> Si substrate which was heated to a temperature of 100°C. The Ti was first evaporated onto the substrate and Al followed during a single evacuation of the vacuum chamber.

The Ti was deposited to a thickness of 600 and 1200Å, while an Al thickness of approximately 15,000Å was used in this investigation. The substrates were prepared by oxidizing the Si surface to form a 3000Å SiO_2 layer which was selectively etched using photolithographic techniques to form Si contact windows which ranged in size from 4 micrometers x 4 micrometers to over 100 micrometers on a side. The metal layer was then deposited over the substrate and heat treated. No metal pattern was used so that Si migration from the contact window to the surrounding areas was not restricted by metal geometry in the film plane. This represents the worst case for Si pit formation in the concact areas since generally metal geometry restricts the extent to which Si may migrate. The samples were heated in a N_2 atmosphere in a three zone furnace accurate to $\pm$ 2°C.

The SEM samples were prepared by randomly cleaving a patterned slice of metalized silicon after heat treatment. The metal was entirely removed in some cases, while in others only the Al was removed by using a selective Al etchant. The sample illustrating Al in the contact hole pit was cleaved in liquid nitrogen to preserve the Al shape during substrate fracture. Electron microprobe samples were prepared in a similar manner to the SEM samples.

CHAPTER III

GROWTH RATE AND STRUCTURE OF THIN FILM Pd_2 Si LAYERS

In this chapter the composition, growth kinetics and structure of Pd_2 Si is described. The Pd_2 Si is formed by low temperature heat treatment of a Pd-Si couple consisting of a thin film layer of Pd deposited on a Si substrate.

The backscattering analysis techniques are first developed and then applied to the investigation of the rate of growth and composition of Pd_2 Si. The study of this system by backscattering techniques is not only useful for device fabrication, but also provides a relatively simple system to develop the analytical techniques which are used in the more complex Si-Ti-Al system described in the next chapter.

The structure of the thin film silicide layer is investigated by means of x-ray diffraction analysis. Powder diffraction analysis is used to identify the silicide as Pd_2Si, while diffractometer and Pole figure analysis are used to determine orientation effects. The film is found to be a highly oriented, uniform layer of Pd_2 Si.

A. Backscattering Analysis Technique

The rate of formation and the composition of the palladium silicide phase was measured by means of 2-MeV $^4He^+$ ion backscattering. The energy spectrum of backscattered ^4He particles provides mass, depth and composition information on the system studied. Such an energy spectrum for a Pd-Si structure is shown in Fig. 3. The sample initially consisted of 3000Å evaporated Pd on a Si single crystal

Fig. 3 Energy spectrum for 2 MeV ^{4}He ion scattering from a Si-Pd sample heated at 250°C for 30 minutes. The initial Pd thickness was 3000Å. The vertical lines indicate the energy positions at the half height points of the different steps in the spectrum.

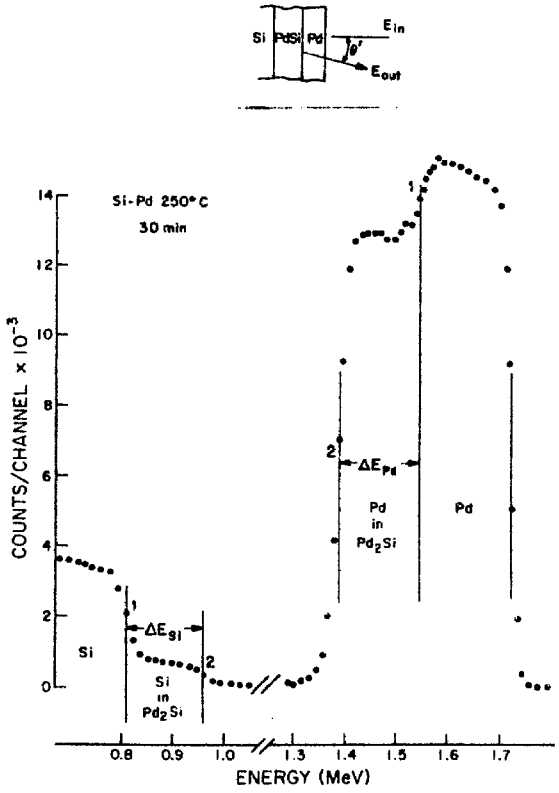
Si
PdSi
Pd
E_{in}
θ'
E_{out}
Si-Pd 250°C
30 min
COUNTS/CHANNEL x 10^{-3}
14
12
10
8
6
4
2
0
1
2
ΔE_{Si}
Si
Si
in
Pd_2Si
ΔE_{Pd}
Pd
in
Pd_2Si
Pd
0.8
0.9
1.0
1.3
1.4
1.5
1.6
1.7
ENERGY (MeV)

Figure 3

substrate. Heat treatment at 250 C for 30 minutes resulted in a palladium silicide layer formed between the Si substrate and the metal.

The energy spectrum in Fig. 3 has two well separated components: one at higher energies due to scattering from Pd and one at lower energies due to scattering from Si. This separation into two regions is a result of the different energy loss experienced by the ^{4}He particles when scattered from species with different masses. More specifically, the maximum energy in the spectrum for an element with mass M will be $E_{max} = k_M E_o$, where k_M is the kinematic recoil factor for ^{4}He ion scattering from an atom with mass M and E_o is the beam energy.

The ^{4}He ions experience energy loss during their inward and outward trajectories in the specimen and thus the energy distribution for scattering from atoms in a thick target specimen will be spread over a range of energies less than E_{max} for the element of interest. In the Appendix a relation between energy of backscattered particles and depth t in the substrate is derived. The detected energy E is approximately $E = E_{max} - [S]t$, where $[S]$ is the backscattering energy loss parameter. For Pd_2Si films up to 5000A thick, the components of the two species are well separated with a ^{4}He beam of 2 MeV at a scattering angle θ ($\theta = 180° - \theta'$) of 170°. For thicker films, the different portions of the spectrum may overlap in energy, and lead to an ambiguous interpretation.

In both components of the energy spectrum in Fig. 3, there is a step in yield which results from the compositional change from pure material to the silicide (see Appendix). The energy widths ΔE of these steps can directly be related to the thickness of the silicide

layer. The number of atoms/cm^2, $N\Delta t$, for a given species is measured from the energy loss ΔE in the silicide, i.e. $\Delta E = [S]/N(N\Delta t)$, where $[S]$ is the backscattering energy loss parameter and N is the atomic density of the film and Δt is the film thickness. For the film thicknesses used in this study ($\Delta t < 5000$Å) the value of $[S]$ varies less than 5% over the layer so ΔE can be treated as a direct measure of film thickness provided the density of the film remains constant with depth. Thus the number of atoms per cm^2 in the silicide region is measured by estimating the energy loss ΔE_{Si} or ΔE_{Pd} (see Fig. 3) in the portion of the spectrum corresponding to the silicide layer. For convenience the values of $(N\Delta t)$ are given in Å using bulk density value of 7.1×10^{22} atoms/cm^3 for the density of Pd_2Si. The energy loss ΔE should be measured as the full width at half maximum of the contribution from the silicide (points 1 and 2 in Fig. 3).[13]

The composition ratio of the two species in the palladium silicide layer may be measured by either of the two methods below. The first method may be used to estimate the composition as a function of depth, while the second method yields the average composition of the entire silicide region.

The ratio of the number of Pd atoms per unit volume (N_{Pd}) to that of Si atoms (N_{Si}) at a depth t in the silicide layer may be calculated by means of the relationship given in the Appendix, Eq. (7):

$$\frac{N_{Pd}}{N_{Si}} = \frac{H_{Pd}}{H_{Si}} \times \frac{[S]_{Pd}}{[S]_{Si}} \times \frac{\left(\frac{d\sigma}{d\Omega}\right)_{Si}}{\left(\frac{d\sigma}{d\Omega}\right)_{Pd}} \qquad (1)$$

H_{Pd} and H_{Si} are the heights in the backscattering spectrum corresponding to Pd and Si respectively. The backscattering yields H_{Si} and H_{Pd} must each be evaluated at the energy corresponding to the same depth t in the film, utilizing the different values of the parameter [S] for Pd and Si respectively. The relevant values of the backscattering parameter [S] and the scattering cross section are given in Table I.

An alternative method which yields an average value of the composition is also discussed in the Appendix, Eq. (14). The following relationship entailing the integrated number of counts A_{Si} and A_{Pd} from each species within the compound is then used:

$$\frac{N_{Pd}}{N_{Si}} = \frac{A_{Pd}}{A_{Si}} \times \frac{\left(\frac{d\sigma}{d\Omega}\right)_{Si}}{\left(\frac{d\sigma}{d\Omega}\right)_{Pd}} \qquad (2)$$

B. Composition and Kinetics of Palladium Silicide Formation

Backscattering of 2-MeV ^4He ions was used to measure the composition and kinetics of the formation of palladium silicide. Figure 4 shows backscattering energy spectra for samples with 3000Å of Pd evaporated onto n-type <100> Si substrates. The samples were heated for 5, 15, and 30 minutes at 250°C and 5, 10 and 15 minutes at 275°C. A single step in both the Si and Pd spectra for all of the samples shown indicated that only one compositional silicide phase was present within the resolution of the system (~200Å). The yield in the silicide regions slowly increases with decreasing energy as is especially apparent in the Pd spectrum. Such a variation in yield is expected in a region of approximately constant composition because of the energy dependence in the cross section and to a lesser degree

TABLE I [a]

Energy (MeV)	$[S]^{Si}_{Si}$	$[S]^{Pd_2Si}_{Si}$	$[S]^{Pd}_{Pd}$	$[S]^{Pd_2Si}_{Pd}$	$\frac{\left(\frac{d\sigma}{d\Omega}\right)_{Pd}}{\left(\frac{d\sigma}{d\Omega}\right)_{Si}}$
2.0	46	100	120	107	11.2
1.8	50	103	125	112	

[a] Values of stopping powers were obtained from J.F. Ziegler and W.K. Chu (submitted to J.A.P.).

Table I gives the values of the backscattering energy loss parameter [S] (eV/Å) and the cross-section ratio $\left(\frac{d\sigma}{d\Omega}\right)_{Pd}/\left(\frac{d\sigma}{d\Omega}\right)_{Si}$ used in evaluating the composition and kinetics of palladium silicide layers (a Pd/Si ratio of 2/1 was used). As introduced in the Appendix, the subscript on [S] refers to the species from which scattering is considered and the superscript refers to the medium in which the energy loss is experienced. The parameters are given for an incoming beam of 2.0 MeV ^{4}He ions and again for 1.8 MeV representing the energy loss of the beam in a ~ 3000Å palladium silicide layer. A scattering angle of 170° was used.

Fig. 4 Energy spectra for 2 MeV ^{4}He ion scattering from Pd-Si samples heat treated for different times at 275°C (upper portion) and 250°C (lower portion). The initial Pd thickness was 300Å.

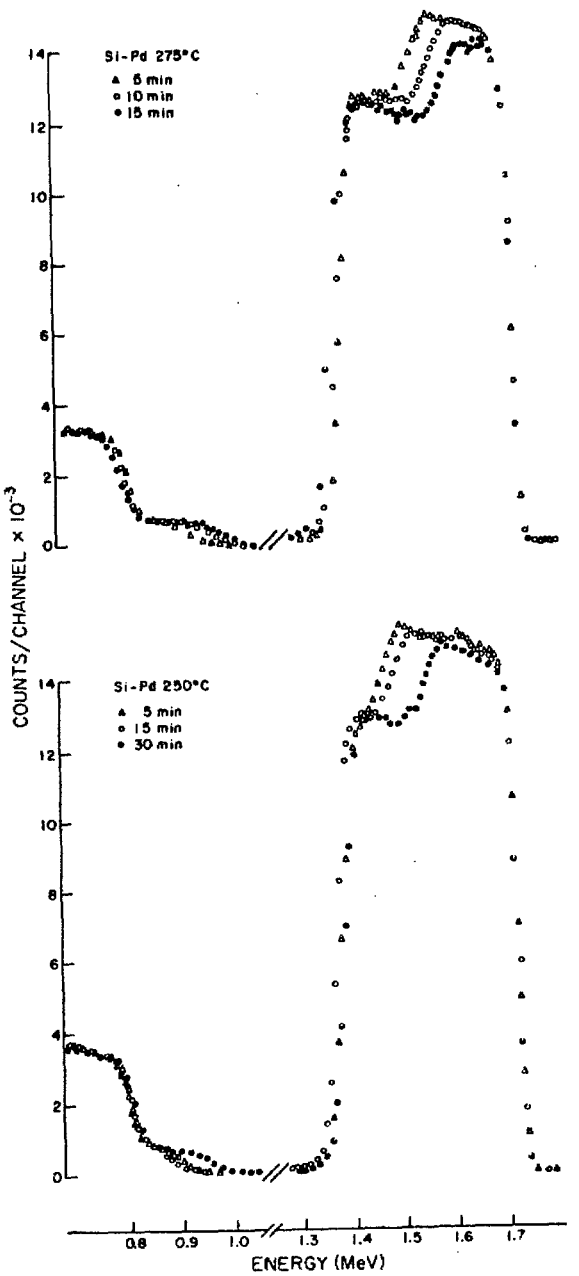
Si-Pd 275°C
▲ 5 min
○ 10 min
● 15 min
Si-Pd 250°C
▲ 5 min
○ 15 min
● 30 min
COUNTS/CHANNEL × 10⁻³
ENERGY (MeV)
0.8
0.9
1.0
1.3
1.4
1.5
1.6
1.7

Figure 4

because of variations in [S] with energy.

1. Composition

The composition of the silicide was measured in samples which were heat treated from 200°C to over 700°C which were formed on both p- and n-type substrates with <111>, <100> and <110> orientation and on amorphous Si layers. No systematic variations in composition were found for any of these cases. The average ratio of Pd to Si was determined from Eq. (1) to be 2.0 ± 0.03 for fully reacted samples with a silicide layer of 1000 to 1500Å. In thicker silicide layers a wider variation in composition was found. This is due in part to the tail (extending in energy below the Pd spectrum) which is superimposed on the silicon signal.[28] This tail increases with increasing thickness of the Pd layer. Pulse pile-up effects may also influence the measured height of the Si step. The composition was determined using the measured energy losses to estimate the quantity

$$[S]_{Pd}^{Pd_2Si} \Big/ [S]_{Si}^{Pd_2Si} = \Delta E_{Pd} \Big/ \Delta E_{Si} = 1.05 \pm 0.05 \quad .$$

This ratio is in the range calculated from values in Table I. The backscattering measurement only identifies composition and not the structure of the silicide layer. The x-ray analysis presented later in this investigation identifies the layer as a single phase of Pd_2Si.

2. Kinetics

Spectra similar to the six shown in Fig. 4 were used to estimate the rate of formation of the silicide layer. In Fig. 5 the square of the rate of energy loss ΔE in the silicide is plotted versus heat

Fig. 5 The figure shows the square of the energy loss ΔE in the silicide region (left scale) and the corresponding Pd_2Si thickness (right scale) as function of heat treatment time. Data points for 4 temperatures and a variety of Si substrates are presented. The horizontal scale is segmented at two points.

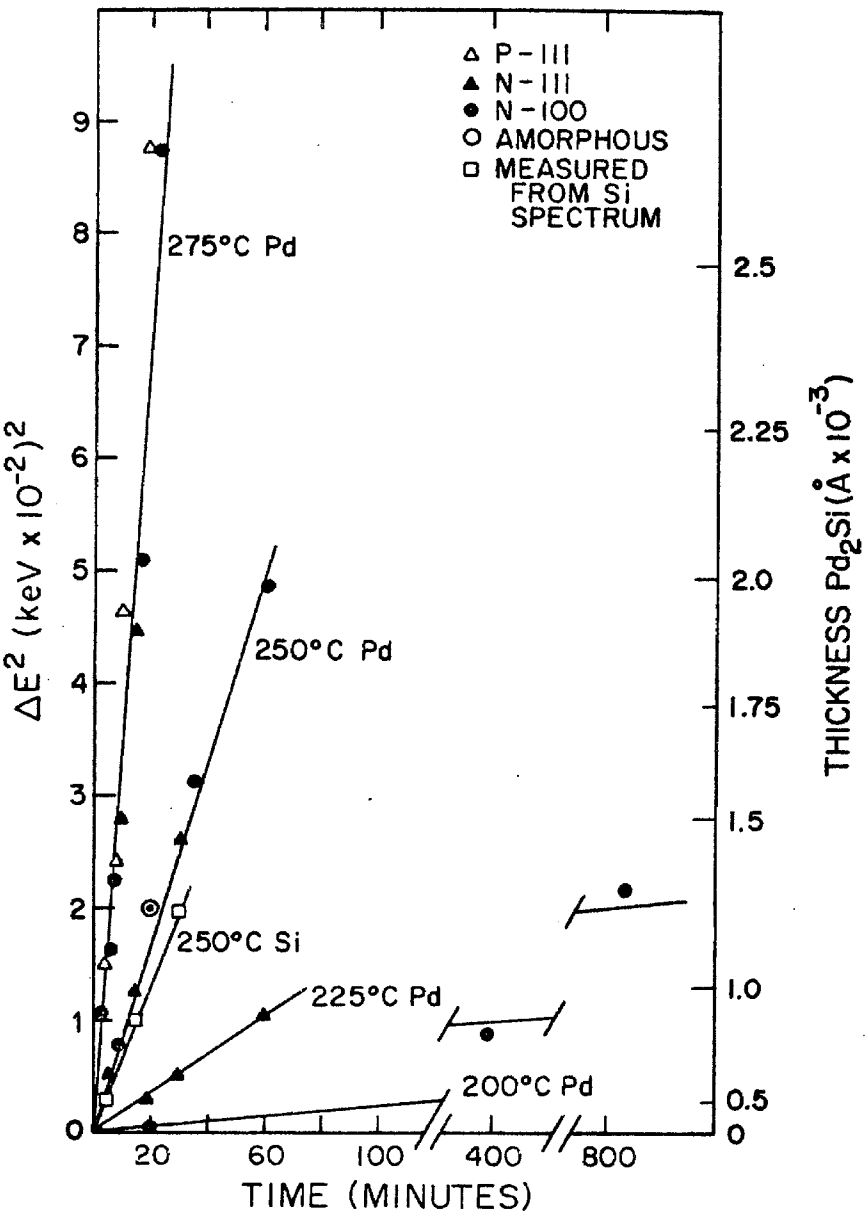
P-III
N-III
N-100
AMORPHOUS
MEASURED FROM Si SPECTRUM
275°C Pd
250°C Pd
250°C Si
225°C Pd
200°C Pd
ΔE² (keV x 10⁻²)²
THICKNESS Pd₂Si (Å x 10⁻³)
TIME (MINUTES)
0
1
2
3
4
5
6
7
8
9
0
0.5
1.0
1.5
1.75
2.0
2.25
2.5
20
60
100
400
800

Figure 5

treatment times for sample heated at 200, 225, 250, and 275°C. The data points shown are for energy loss in the palladium portion of the silicide spectrum ΔE_{Pd}, except for the three points shown for silicon in the silicide at 250°C. Since film thickness is proportional to energy loss, a straight line on this graph represents the case where the square of silicide film thickness increases proportionally with time. This growth dependence generally results when the diffusion of the species through the film limits the process.[29] The straight lines shown represent the best fit through the origin to the data points at each temperature. The heat treatment times are known to better than $\pm$ 1 minute and the estimated error in E^2 due to this uncertainty is .05 (Kev x $10^{-2})^2$. Thus the data symbols shown exceed the margin of experimental error for these parameters. The process temperature, however, was known to only $\pm$5°C which would account for data spread from the straight lines considerably exceeding that shown in this figure. The horizontal scale is segmented at two points to allow the 200°C data points to be shown after 395 and 805 minutes of heat treatment.

The kinetics data presented were taken from evaporated Pd samples prepared on both n- and p-type Si single crystal substrates of <111> and <100> orientation and on amorphous substrates. The rate of formation of the Pd_2Si does not appear to depend upon any of these parameters. The rate of formation was, however, affected by an oxide interface layer between the Si and Pd. In the case of an oxide interface produced by boiling the wafer in H_2O prior to the Pd evaporation, the onset of Pd_2Si formation appeared to be delayed for

several minutes whereupon the silicide grew at the same rate as when no oxide was initially present. The rate constants determined from the slope of the four lines shown in Fig. 5 are presented as a function of reciprocal temperature in Fig. 6. The four points fall approximately on a straight line which represents a single activation energy for the silicide formation in this temperature range. Analysis of this curve yields an activation energy E_a of 1.5 ± 0.1 eV.

C. X-Ray Diffraction Analysis

The ^{4}He backscattering results indicated that a film of composition near Pd_2Si results when a Pd layer evaporated onto Si is heated in the temperature range of 200 to 700°C. X-ray diffraction analysis was used to identify structurally the resulting film and to determine its orientation with respect to the substrate material on which it was formed. Debye-Scherrer powder diffraction was used to identify the structure, while pole figures were constructed to determine orientation effects.

1. Structural Identification of Pd_2Si

The measured x-ray intensities from the powder specimen prepared from the thin silicide films are given in the left column of Table II. These data compared well with either of the Powder Diffraction File listings for Pd_2Si, which are 6-559 and 19-893.[30,31] While the weak super-lattice lines of the latter were not detected, the lines which were detectable matched substantially better with 19-893. Thus the structural identification is made with Pd_2Si (19-893). Comparison of the data is provided in Table II, which lists all planar spacings greater than 1.55A and relative intensities greater than 30 are listed for Pd_2Si.

Fig. 6 The figure shows the rate constants for Pd_2Si formation determined from Fig. 3 as function of reciprocal temperature. The top scale gives the corresponding temperature values in degrees centigrade.

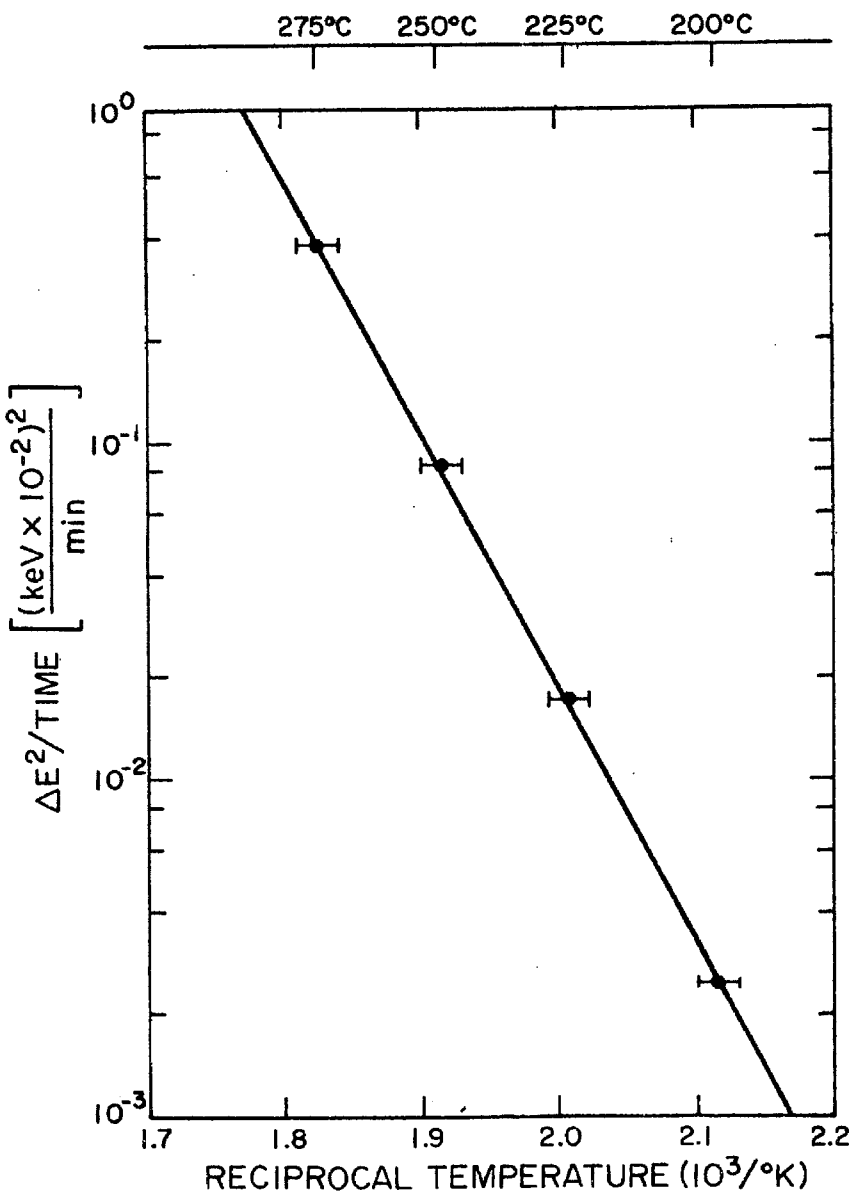
275°C
250°C
225°C
200°C
10^0
10^{-1}
10^{-2}
10^{-3}
$\Delta E^2/\text{TIME}\left[\frac{(\text{keV}\times 10^{-2})^2}{\text{min}}\right]$
1.7
1.8
1.9
2.0
2.1
2.2
RECIPROCAL TEMPERATURE (10^3/°K)

Figure 6

TABLE II

Specimen Measured		PDF 19-893			PDF 6-559		
d(Å)	intensity	d(Å)	I/I_o	<h k.ℓ>	d(Å)	I/I_o	<h k.ℓ>
3.27	weak	3.26	50	220	3.21	30	110
2.955	weak	2.935	40	208			
-		2.811	30	400	2.83	20	200
2.371	strong	2.366	100	228	2.35	100	111
2.187	moderate	2.182	90	408	2.16	80	201
2.141	moderate	2.136	90	240	2.12	80	120
1.885	moderate	1.884	80	600	1.87	60	300
1.82	weak	1.815	50	248	1.80	30	121
1.721	strong	1.718	60	0016	1.71	50	002
1.55	weak	1.569	50	50	1.56	30	310

Table II presents a comparison of the measured d-spacing and their intensities with the two forms of Pd_2Si listed in the Powder Diffraction File (PDF).

The preferred orientation of the powder specimen apparently led to the strong 00.16 reflection corresponding to a plane spacing of 1.72Å and the absence of the 40.0 reflection at 2.81Å. No unexplained reflections were noted, indicating that a single phase of Pd_2Si forms, which is in agreement with other reported work.[6,7]

2. Orientation of Pd_2Si

Diffractometer measurements of Pd_2Si films as formed on the various substrates showed the films to have a high degree of preferred orientation. The {00.16} Pd_2Si reflection was dominant by far over all other reflections for all specimens, although the degree of preferred orientation depended upon the substrate orientation. The preferred orientation is highest for the <111> Si substrate, and least (although still strong) for the substrate with an amorphous film. This indicates a strong tendency for Pd_2Si to grow with the hexagonal basal plane parallel to the substrate surface regardless of the crystalline orientation of the substrate. The high degree of orientation reported here for Pd_2Si formed on <111> Si has also been noted by other investigators.[7]

In order to study more closely the degree of orientation of the films, pole figures were constructed for the {00.16} and {22.8} Pd_2Si reflections. The {00.16} poles show the orientation distribution of the c-axis of the numerous Pd_2Si crystallites in the film which were mainly perpendicular to the substrate surface; the {22.8} poles show in addition the degree of rotational alignment of the crystallites about the c-axis.

The results are summarized in Fig. 7. Each part of the figure is a stereographic projection showing schematically the distribution of the {00.16} and {22.8} Pd_2Si poles, superimposed upon the poles of

Fig. 7 Results of pole figure analysis on Pd_2Si layers formed on Si substrate of various orientations. The left side of the figures gives the distribution of poles, while the two columns of figures on the right side are measured angular widths of the $\{22.8\}$ poles. The samples were heat treated at 400°C for 30 minutes.

POLE FIGURES

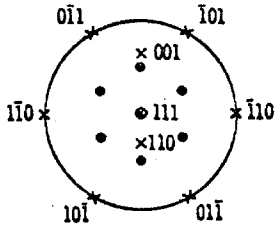

	$(\Delta x)_{FWHM}$	$(\Delta\phi)_{FWHM}$
(a) ⟨111⟩ Si	1.3°	1.4°

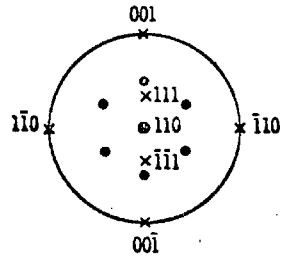

(b) ⟨110⟩ Si	8.5°	27°

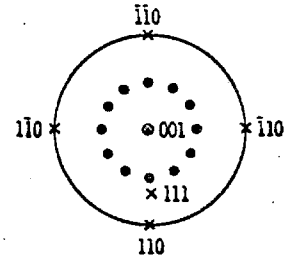

(c) ⟨100⟩ Si	11.5°	16°

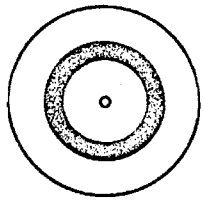

(d) AMORPHOUS Si	19°	—

● {22.8} Pd_2Si

○ {00.$\underline{16}$} Pd_2Si

× Si AS MARKED

Figure 7

the Si substrate. Each part represents one Si substrate orientation type, and the locations of the Si (001), (110) and (111) poles are shown in each (except the amorphous Si substrate). The Si pole at the center of each stereographic projection is, of course, the orientation of that substrate. Note that the Si lattice in the substrate for 7(b) may be obtained from 7(a) by tilting the Si lattice upward by 35.3° about an axis through $(\bar{1}10)$ and $(1\bar{1}0)$, while 7(c) may be obtained from 7(a) by tilting downward 54.7° about the same axis.

The pole figures show that the $\{00.\underline{16}\}$ Pd_2Si pole is concentrated at the center of each stereographic projection, i.e., the Pd_2Si c-axis prefers to be perpendicular to the substrate for all substrate types. The full widths at half-maximum (FWHM) of the distributions are shown in Table III. These values have been corrected for instrumental resolution. These distribution widths demonstrate quantitatively the diffractometer results above, namely the substantial degree of preference according to substrate type, with the [111] case the highest degree of orientation and the amorphous substrate the least with the [110] and [001] cases about halfway between the extremes.

The $\{22.8\}$ pole distributions show a similar decrease in degree of preferred orientation. The corrected typical FWHM's in azimuthal angle χ and in polar angle ϕ are tabulated in Fig. 7; $(\Delta\chi)_{FWHM}$ for the $\{22.8\}$ shows the same trend with substrate type as for the $\{00.\underline{16}\}$.

A qualitative description of the preferred orientation of the Pd_2Si films consistent for all substrates is that:

a) The hexagonal basal plane is always parallel to the substrate surface.

TABLE III

Si Orientation	$\Delta(\chi)_{FWHM}$
<111>	1.3°
<110>	10.5°
<100>	10.5°
Amorphous	18°

Table III gives the angular width $(\Delta\chi)_{FWHM}$ of the (00.16) reflection in Pd_2Si samples formed on Si substrate with different orientations. The samples were heated at 400°C for 30 minutes.

b) A $\{20.0\}$ Pd_2Si pole lines up with any diametrically opposite pair of <110> Si directions (such as $[1\bar{1}0]$ and $[\bar{1}10]$ in the plane of the substrate. The $\{20.0\}$ poles are halfway in polar angle between the $\{22.8\}$ poles in a standard (00.1) projection.

Thus, for the [111] Si substrate, the $\{22.8\}$ Pd_2Si pole figure lines up simultaneously with all three <110> Si pairs in the plane of the substrate. For [110] Si there is one such pair. However, for [001] Si, there are two such pairs at right angles. Then there appears to be a superposition of two $\{22.8\}$ pole figures, each aligned to a <110> Si pair, with the resulting apparent doubling in the number of $\{22.8\}$ poles.

For an amorphous substrate there is no rotational preference, and the Pd_2Si 22.8 poles are spread out over 360°, even though the Pd_2Si $\{00.\underline{16}\}$ shows a marked preferred orientation.

Added insight into these orientation effects in Pd_2Si films is provided by ^4He ion channeling techniques which are included in the Appendix.

CHAPTER IV

GROWTH RATE AND STRUCTURE OF $TiAl_3$ FORMED FROM THIN FILM LAYERS OF Ti-Al DEPOSITED ON Si

In this chapter the composition, growth rate and structure of $TiAl_3$ is described. The $TiAl_3$ is formed by a low temperature heat treatment of an Al-Ti-Si system consisting of thin films of Ti and Al deposited on a Si substrate.

The backscattering spectrum resulting from bombardment of this system with 2-MeV ^4He ions is much more complex than the Pd-Si case described in the last chapter. However, the same basic analysis techniques developed in the last chapter to detect formation and measure the rate of growth and composition of compound layers may again be used for the Al-Ti-Si system. The rate of formation of $TiAl_3$ from thick couples of Ti-Al and Ti-AlTi has recently been reported.[32] The $TiAl_3$ layers measured were formed upon heating to temperatures ranging from 516 to 642°C resulting in aluminide layers of tens to hundreds of microns in thickness. The structures of interest for semiconductor application described in the next chapter are much thinner and the process temperatures lower. Hence, the work in this chapter relates to film thicknesses and process temperatures applicable to semiconductor applications. The results for the two cases proved to be quite different.

The structure of $TiAl_3$ and subsequent development of a Si rich ternary phase of Ti-Al-Si is investigated by means of x-ray diffraction and electron microprobe analysis. The consumption of the

Ti layer in the formation of $TiAl_3$ and subsequent formation of the Si rich ternary is found to be the key to understanding and controlling the failure mechanism found in Ti-Al contacts to Si described in chapter V.

A. Composition and Kinetics of $TiAl_3$ Formation

Backscattering of 2 MeV ^4He was used to detect composition and kinetics of phase changes in the Ti-Al-Si thin film system. This system is more complex than the Pd-Si system described in Chapter III because two interfaces are involved and considerable overlap in the energy spectra resulting from the Si, Al and Ti result. The same basic analysis techniques may be used for this system however. The backscattering energy loss parameter, [S], is relatively constant in the various regions of interest in the film allowing depth and compositional scales to be constructed as described in the Appendix. The composition of the Ti-Al compound is determined from the relation

$$\frac{N_{Al}}{N_{Ti}} = \frac{H_{Al}}{H_{Ti}} \times \frac{[S]_{Al}}{[S]_{Ti}} \times \frac{\left(\frac{d\sigma}{d\Omega}\right)_{Ti}}{\left(\frac{d\sigma}{d\Omega}\right)_{Al}}$$

while the rate kinetics is determined from the relation $\Delta E = \left(\frac{[S]}{N}\right)(N\Delta t)$. Both of these expressions were derived and symbols defined previously for the Pd-Si system. Backscattering energy loss parameters for Al, Ti and $Ti-Al_3$ are given in Table IV where Bragg's rule has been used to compute the energy loss parameters in the compound.[27]

1. Composition

The composite energy spectrum for an as deposited Al-Ti film on a Si substrate is shown in figure 8. The Ti layer is approximately

TABLE IV [a]

Energy (MeV)	$[S]^{Al}_{Al}$	$[S]^{TiAl_3}_{Al}$	$[S]^{Ti}_{Ti}$	$[S]^{TiAl_3}_{Ti}$	$\frac{\left(\frac{d\sigma}{d\Omega}\right)_{Ti}}{\left(\frac{d\sigma}{d\Omega}\right)_{Al}}$
2.0	45.8	56.8	78.6	58.7	2.95
1.8	46.8	58.2	81.9	61.6	

[a] Values of the stopping powers were obtained from J.F. Ziegler and W.K. Chu (submitted to J.A.P.).

Table IV gives the values of the backscattering energy loss parameter [S] (eV/Å) and the cross section ratio $\left(\frac{d\sigma}{d\Omega}\right)_{Ti} / \left(\frac{d\sigma}{d\Omega}\right)_{Al}$ used in evaluating the composition and kinetics of $TiAl_3$. The subscript on [S] refers to the species from which scattering is considered and the superscript refers to the medium in which the energy loss is experienced. The parameters are given for an incoming beam of 2.0 MeV ^4He ions and again for 1.8 MeV representing the energy loss of the beam in a ~ 6000Å $TiAl_3$ layer. A scattering angle of 170° was used.

Fig. 8 This figure illustrates the backscattering spectrum from an unreacted Ti-Al film deposited on a Si substrate. A 2 MeV ^4He beam was used to analyze the film. The Al was approximately 10,000Å and the Ti 1200Å in thickness.

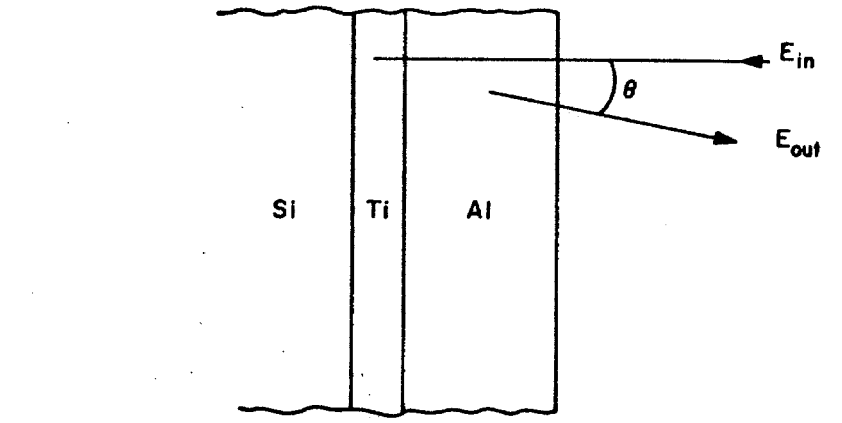
E_{in}
θ
E_{out}
Si
Ti
Al

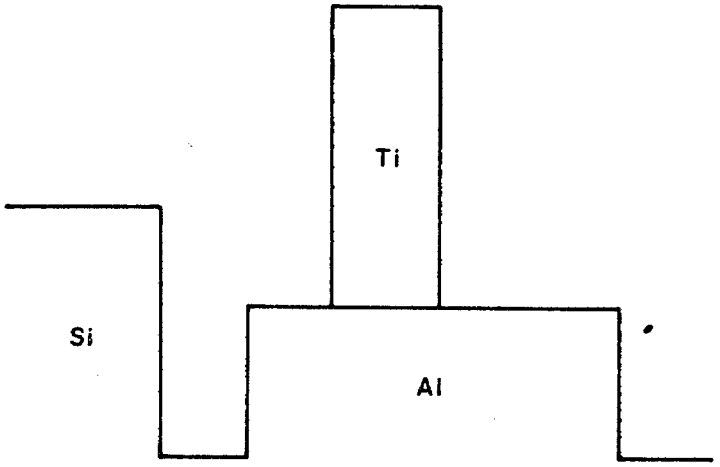
Ti
Si
Al

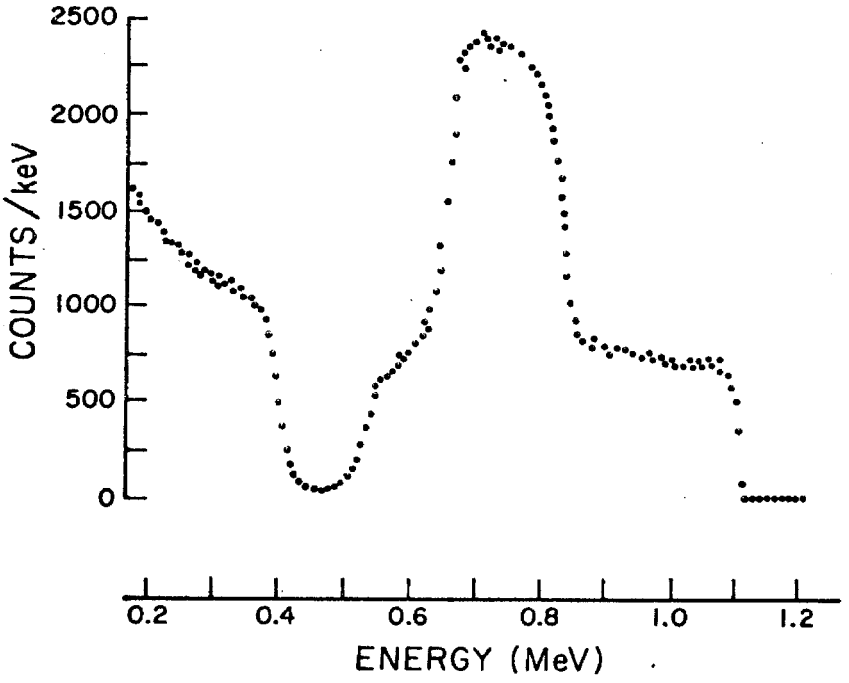
2500
2000
1500
1000
500
0
COUNTS / keV
0.2
0.4
0.6
0.8
1.0
1.2
ENERGY (MeV)

Figure 8

1500Å thick, while the Al thickness is the order of 10,000Å. As shown in the schematic diagram in the center of this figure the energy spectrum from the relatively thick Al surface layer overlaps the spectrum resulting from the underlying Ti. The actual Ti spectrum thus is found by subtracting the Al spectrum from the composite in the region where overlaps occur. The high energy edge of the Ti spectrum and the low energy edge of the Al spectrum result from adjacent material at the Ti-Al interface. The low energy edge of the Ti spectrum and the high energy edge of the Si spectrum similarly result from these substances at the Ti-Si interface.

An Al-Ti film on a Si substrate which has been heated to 400°C for 242 minutes is shown in Figure 9. Analysis of this spectrum reveals several features. First, no apparent change is seen in the low energy Ti edge or the high energy Si edge. This indicates that no silicide phase has developed as a result of the heat treatment.[15] However, a decided shoulder has developed at higher energies than the previous upper edge of the Ti spectrum. Although it is somewhat obscured by the interference of the overlapping Ti spectrum, a shoulder has developed on the low energy portion of the Al spectrum. These shoulders represent significant compositional changes from their pure metal phases.

The ratio of backscattered yield H_{Al}/H_{Ti} was found to be 1.10 $\pm$ 0.05. Using the relation $[S]_{Al}^{Ti\text{-}Al} \Big/ [S]_{Ti}^{Ti\text{-}Al} = \frac{(\Delta E)_{Al}}{(\Delta E)_{Ti}}$, the ratio of [S] factors was estimated from the ratio of energy losses $(\Delta E)_{Al}/(\Delta E)_{Ti} = .95 \pm .025$. The composition ratio of Al to Ti is then given by $N_{Al}/N_{Ti} = 3.1 \pm 0.2$. Backscattering analysis has thus shown that a

Fig. 9 A partially reacted layer of Ti-Al on Si shown in this figure. The backscattered spectrum from the 2 MeV ^4He beam reveals the formation of a $TiAl_3$ layer between the Al and Ti and no reaction at the Si-Ti interface. This sample was heated to 400°C for 242 minutes.

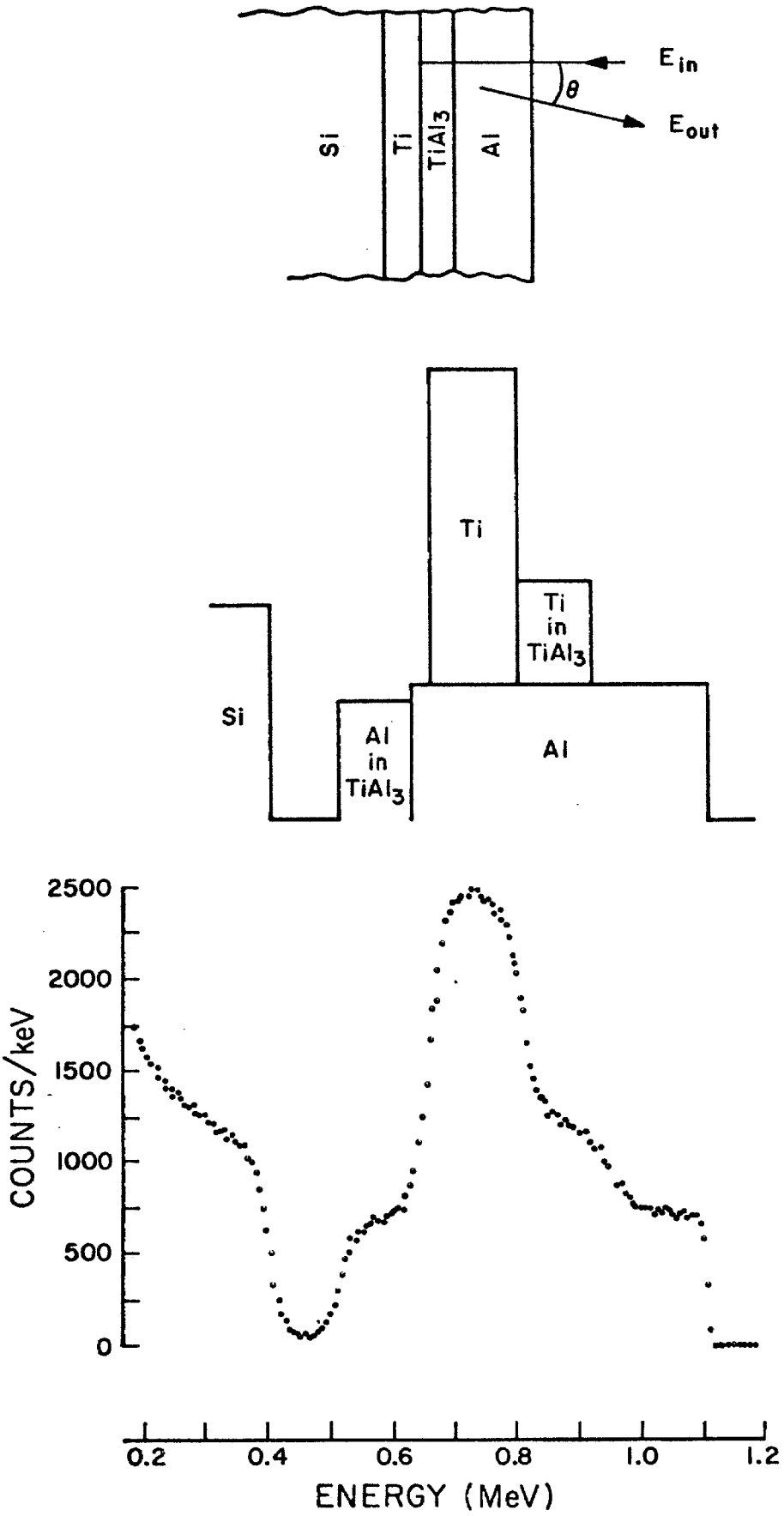
Si
Ti
TiAl3
Al
Ein
θ
Eout
Ti
Ti in TiAl3
Si
Al in TiAl3
Al
COUNTS/keV
2500
2000
1500
1000
500
0
0.2
0.4
0.6
0.8
1.0
1.2
ENERGY (MeV)

Figure 9

material of approximate composition $TiAl_3$ forms in the temperature range of 400 to 500°C while no apparent interaction occurs between the Si and Ti. Thus the Al-Ti reaction does not appear dependent on the presence of the Si. This was confirmed by noting that the energy widths of the ratio of the spectrum resulting from the $TiAl_3$ region was equivalent for samples prepared on Si and SiO_2 substrates and heated to 400°C for 162 minutes.

2. Kinetics

The schematic representation of the Al-$TiAl_3$-Ti-Si spectrum for a partially reacted film in figure 9 illustrates the problem in measuring the rate of $TiAl_3$ formation from the backscattering data. In principle the measurement of the full-width-half-maximum (FWHM) of either the Al or Ti spectrums in $TiAl_3$ as a function of heat treatment would provide the desired kinetics data. In practice, the surface Al layer obscures this measurement. Any nonuniformity in the thickness of the Al layer causes the transitions in the spectra of the underlying regions to be spread in energy.[33] If the Al layer is uniform the transitions in the Ti and Al spectrums resulting from an abrupt change from $TiAl_3$ to Ti and Al occur within an energy range equal to the resolution of the beam and/or detection system (~ 20 KeV). An Al film thickness nonuniformity of approximately 100A or 1% of the total Al thickness will result in approximately this same energy spread. Furthermore, only the Ti spectrum may used to measure the aluminide formation since the spectrum from the unreacted Al is nearly equal in yield to the Al in the $TiAl_3$ layer and completely obscures the energy loss measurement in the Al portion of the spectrum.

It has been found that the Al surface layer can be selectively removed in a chemical etchant, consisting of 40 parts H_2PO_3, 2 parts HNO_3, 9 parts H_2O. At room temperature this etchant removes approximately 1000Å of Al per minute and less than 50Å of $TiAl_3$ in the same period of time. A distinct color change occurs when the Al layer is removed so the material can be easily removed from the etchant with less than 50Å of $TiAl_3$ removed. This was determined on selected samples by measuring the change in the spectrum resulting from 10 minutes in this etchant.

When this process is applied after heat treatment the energy loss in the $TiAl_3$ layer can be easily measured. This is illustrated in figure 10 for a sample which was heated to 400°C for 242 minutes prior to etching. Once the surface Al layer is removed the energy width (FWHM) of the Al in the $TiAl_3$ may be directly measured since its portion of the spectrum is completely isolated from other regions. The Al spectrum now provides the most direct measure of the $TiAl_3$ thickness. Thus, by measuring the FWHM of the Al in $TiAl_3$ spectrums as a function of the time and temperature of heat treatment, the $TiAl_3$ growth kinetics can be determined from the energy loss relationship. This procedure is illustrated in Figure 11.

A series of three spectra are shown in figure 11 which were heated to 400°C for 122, 242, and 374 minutes from bottom to top in this figure. In this sequence all the samples were prepared on a Si substrate. The three Al in $TiAl_3$ spectrums are superimposed at the top of this figure with the energy losses ΔE_1, ΔE_2, and ΔE_3 shown. Since the $TiAl_3$ layer is now at the surface the upper energy is now measured from a common point $E_{max\ Al} = K_{Al}\ E_{in}$, where K_{Al} is the kinematic

Fig. 10 The unreacted Al has been chemically etched from this sample of Al-Ti on SiO_2 after a heat treatment of 400°C for 242 minutes. The Al spectrum in the Ti compound may be directly measured in this case. The incoming beam was 2 MeV ^4He.

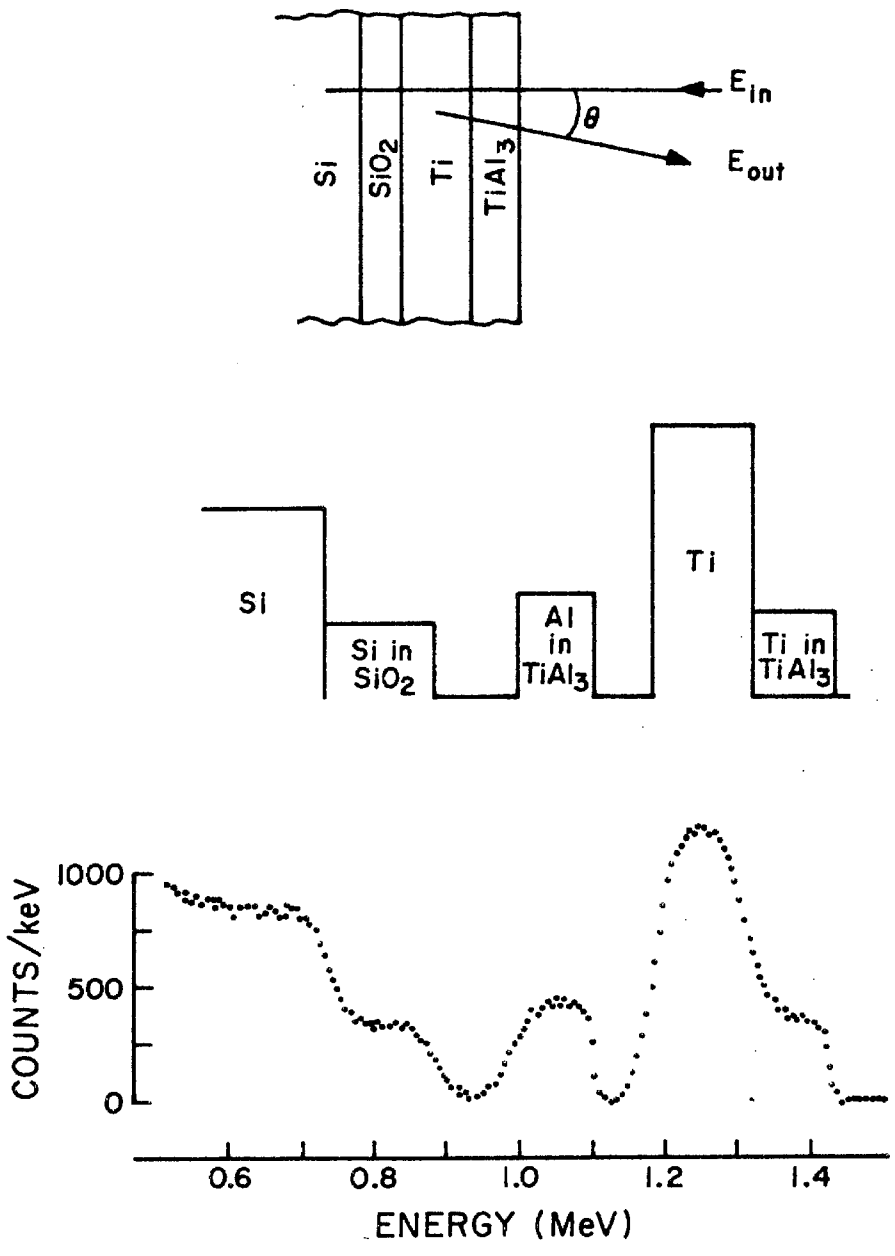
Si
SiO2
Ti
TiAl3
Ein
θ
Eout
Si
Si in SiO2
Al in TiAl3
Ti
Ti in TiAl3
COUNTS/keV
1000
500
0
0.6
0.8
1.0
1.2
1.4
ENERGY (MeV)

Figure 10

Fig. 11 A sequence of three spectra are shown for samples of Al-Ti deposited on Si which were heated for successivly longer times from the bottom to the top. The samples were heated for 122, 242, and 374 minutes at 400°C. The three Al in $TiAl_3$ spectra are superimposed at the top of this figure. The high energy edge of all three Al spectra are at 1.105 MeV which corresponds to 2 MeV ^4He backscattering from Al at the surface of the film. Similarly, the upper energy edge of the three Ti spectra at 1.43 MeV corresponds to surface Ti.

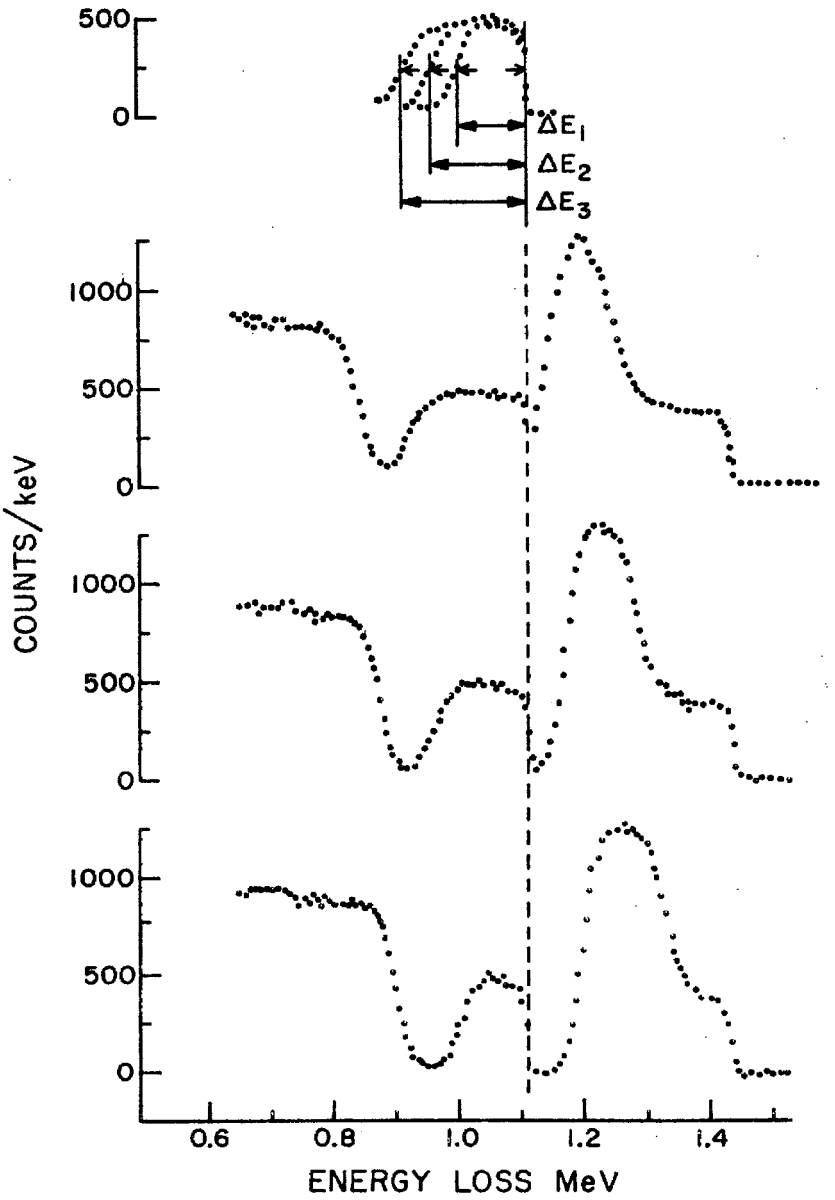
500
0
ΔE1
ΔE2
ΔE3
1000
500
0
1000
500
0
1000
500
0
COUNTS/keV
0.6
0.8
1.0
1.2
1.4
ENERGY LOSS MeV

Figure 11

recoil factor for Al at $(\theta-\theta')=170°$ and E_o =2 MeV. The composition of Al to Ti can also be readily measured from these spectrums to confirm the earlier conclusion that $N_{Al}/N_{Ti} \approx 3$.

The energy loss, ΔE, in the Al spectrums of $TiAl_3$ was measured for a number of periods of heat treatment at each of four temperatures. It was determined that at each temperature the square of the energy loss is approximately proportional to the time of isothermal heat treatment. Since the energy loss, ΔE, is proportional to film thickness, Δt, this corresponds to a rate formation of $TiAl_3$ (proportional to $(\text{time})^{\frac{1}{2}}$. This is the limiting form of rate kinetics in which the flux of material across the $TiAl_3$ product layer itself limits the rate of growth of the Aluminide layer.

In figure 12 the square of the energy loss is plotted versus the period of time that the sample was heat treated for each of the four temperatures measured. The data points shown were used to determine the least square fit straight line shown for each temperature. The time of heat treatment is known in the worst case to within $\pm$ 3 minutes and ΔE^2 has an uncertainty of 0.4×10^{-3} keV^2 introduced by the finite resolution of the detector and noise in the electronics. The data symbols shown slightly exceed the range of uncertainty in each of the variables and thus the scatter in the data is somewhat larger than might be expected especially at 425°C and 450°C. However, the temperature uncertainty in the furnace used is $\pm$ 2°C which would result in a variation of $\pm$ 10% in the slope of each line. This variation in slope is large enough to account for the data scatter shown. A scale corresponding to the approximate thickness of Ti consumed is shown on the right ordinate of this figure. This scale was derived from energy loss measured in totally reacted $TiAl_3$ layers

Fig. 12 This figure illustrates the growth rate of $TiAl_3$. Energy loss in the Al spectrum of $TiAl_3$, which is proportional to thickness, is displayed for samples heated to 400, 425, 450 and 475°C. The least square fit straight lines drawn for each temperature represent transport limited growth since $(\text{energy loss})^2$ is plotted versus time. An approximate scale of Ti consumed in the $TiAl_3$ formation is shown on the right side of this figure.

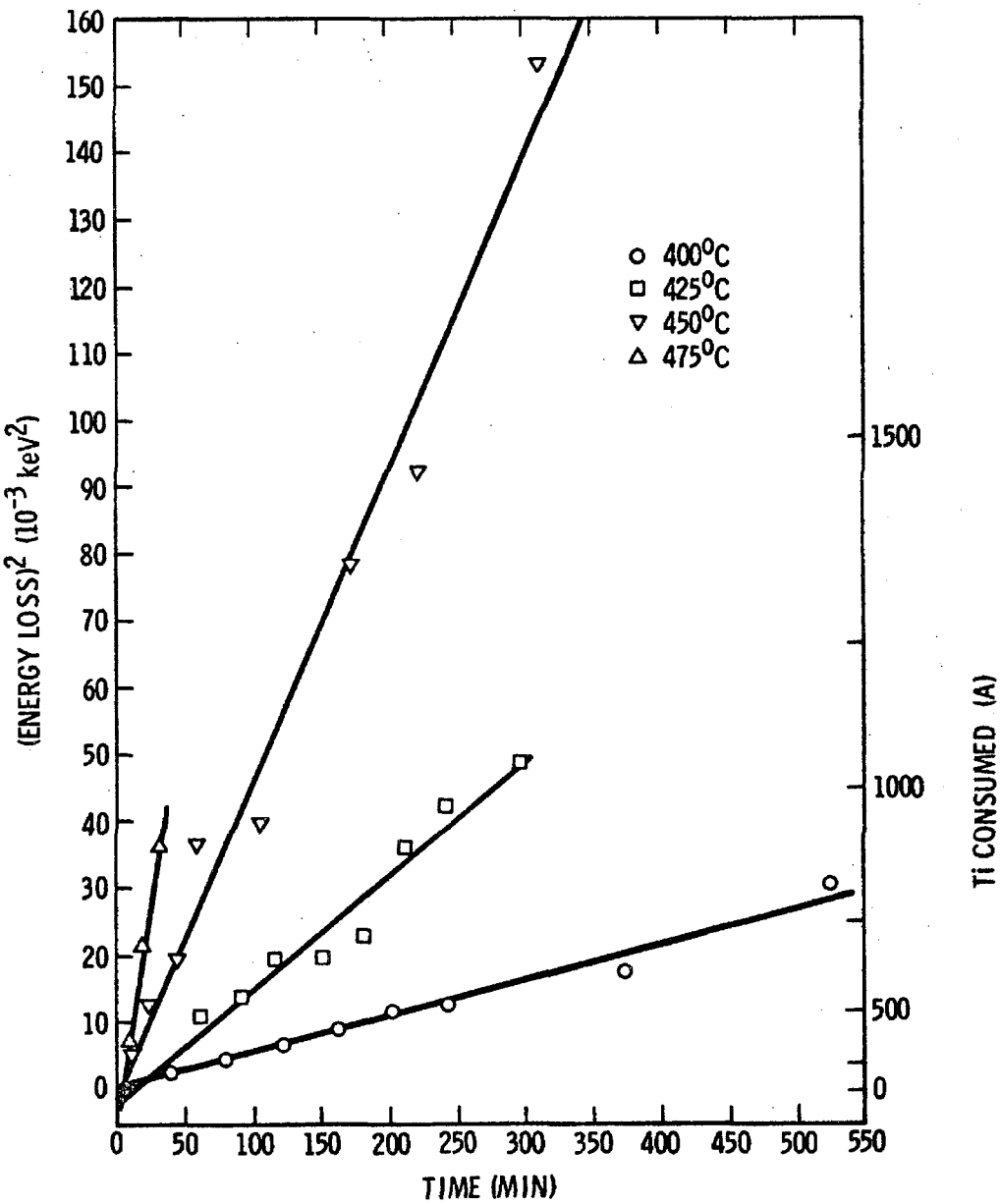
160
150
140
130
120
110
100
90
80
70
60
50
40
30
20
10
0
(ENERGY LOSS)^2 (10^{-3} keV^2)
400°C
425°C
450°C
475°C
1500
1000
500
0
Ti CONSUMED (A)
0
50
100
150
200
250
300
350
400
450
500
550
TIME (MIN)

Figure 12

corresponding to known initial thicknesses of Ti. The scale also corresponds closely to calculated consumption of bulk density Ti in forming $TiAl_3$ using the backscattering energy loss factor from Table IV.

An Arrhenius plot of the rate constant, d, at each temperature, which corresponds to the slope of straight lines determined in figure 12, is shown in figure 13. These four data points fit a single straight line to well within the experimental accuracy shown. The straight line shown in the least square fit to these four points. As indicated previously, the temperature is known to within $\pm$ 2°C indicated by the horizontal error bars. The uncertainty in d at each temperature was estimated from the uncertainty in the slope of each line in figure 12.

The activation energy corresponding to the data in figure 13 is 1.85 $\pm$ 0.05 eV. The rate of consumption of Ti thin film in the formation of $TiAl_3$, X, in cm is given by $X^2=d\tau$, where d=0.15 exp - (1.85/KT) cm^2/sec, and τ is the time in seconds, for the temperature range measured. In applications where Ti consumption is critical such as Ti-Al metal contacts on Si integrated circuits described in Chapter V this expression may be directly used to determine suitable values of Ti thickness and heat treatment to avoid contact failure.[21,22]

The growth rate of $TiAl_3$ found in this work only applies to the 400 to 500°C temperature range and for thicknesses of $TiAl_3$ less than a micrometer resulting from layers of Ti and Al deposited during a single vacuum evacuation. The growth of $TiAl_3$ in the range of tens to hundreds of micrometers in thickness, resulting from pressure formed or hot dipped couples, heated to 516 to 642°C have recently been reported.[32] A linear rate of growth with an activation energy

Fig. 13 An Arrhenius plot of slopes of the four least square lines derived from the growth rate data is shown in this figure. Error bars are shown for both temperature uncertainty and the uncertainty in the slope of growth rate lines. A least square fit of these four points indicates an activation energy of (1.85 ± 0.05)eV.

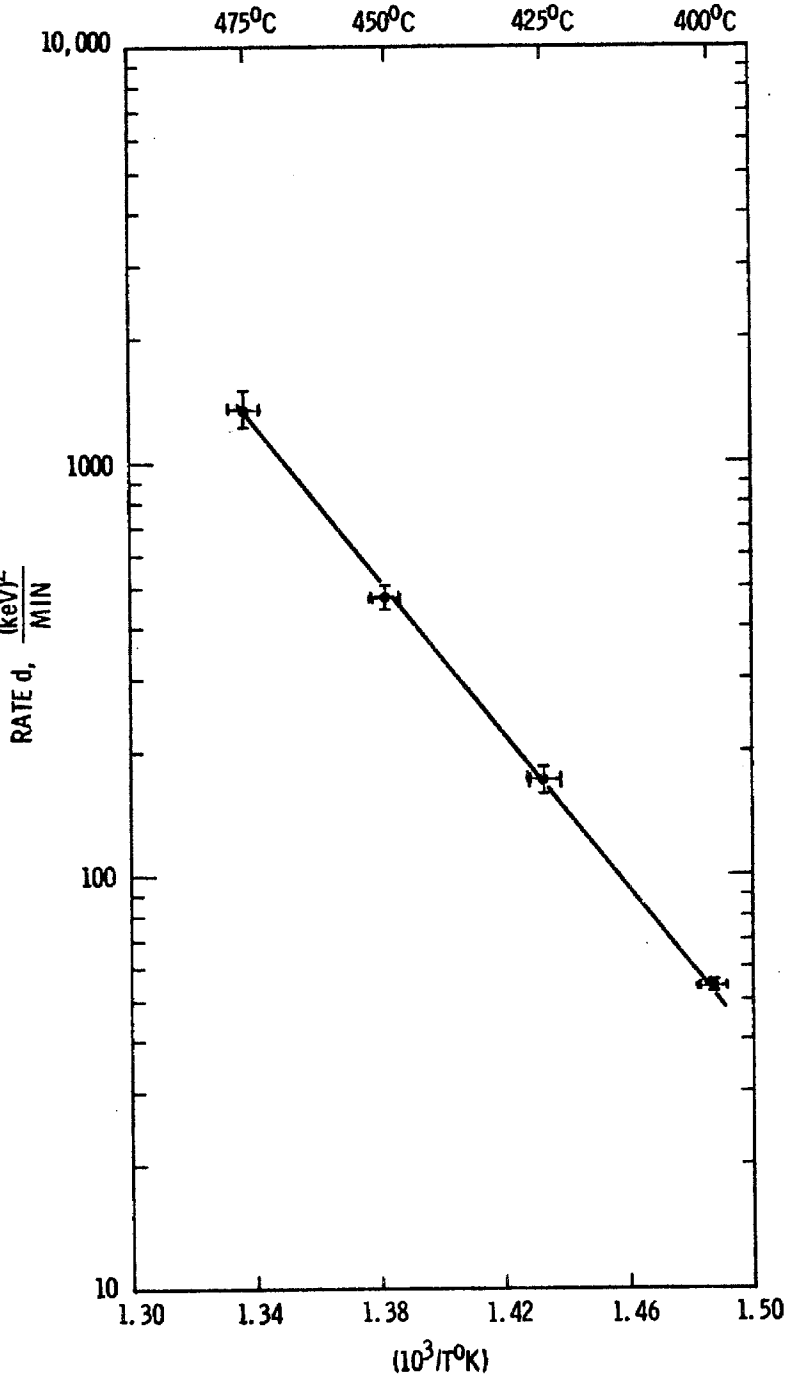
475°C
450°C
425°C
400°C
10,000
1000
100
10
RATE d, (keV)²/MIN
1.30
1.34
1.38
1.42
1.46
1.50
(10³/T°K)

Figure 13

of approximately 1.85 eV, followed by a growth proportional to $(\text{time})^{\frac{1}{2}}$ with an acitvation energy of less than 1 eV is reported for these thick $TiAl_3$ layers.[32] Thus, the present work, which was chosen to match semiconductor metallization process parameters must not be extrapolated to higher temperatures and thicker layers where substantially different results have been found.

B. Structural Analysis of the Ti-Al Layer by X-Ray Diffraction and Electron Microprobe Analysis

Examination of the phase diagram of the binary Ti-Al system indicates several intermetallic phases plus the α phase of Ti which has a solubility range exceeding 30 atomic percent Al.

The Ti-Al layer used to prepare the powder specimen in this investigation consisted of an Al-Ti couple on a Si substrate which was heated to 450°C for 1000 minutes. Based on the rate kinetics for the formation of $TiAl_3$, this time and temperature would have been just sufficient to consume the entire 3000Å layer of Ti contained in this sample. The sample was measured with an electron microprobe and found to be Al rich. Comparison of the x-ray diffraction lines found for this sample with known Al-Ti compounds indicate that the majority of the material in the powder specimen prepared from this specimen is $TiAl_3$.[34,35,36,37]

The details of this comparison are presented in Table V. The measured values for the Ti residual are shown on the left side of the table, while the center and right side delineate the stronger lines of a standard $TiAl_3$ diffraction pattern. The $TiAl_3$ standard shown in this table was taken from the Powder Diffraction File (PDF)

TABLE V

Al Rich Ti Layer		PDF:2-1121 $TiAl_3$			Other Substances	
d(A)	I/Io	d(A)	I/I	(h k ℓ)	d(A)	Comment
4.33	35	4.30	40	002		
3.52	45	3.51	50	111		
3.13	35				3.14	(111) Si
2.27	100	2.30	100	113,202		
2.20	60				2.21	(116) Ti-Al-Si(I/Io=100)
2.13	60	2.15	70	004		
2.02	30				2.03	(01 $\underline{11}$)Ti-Al-Si(I/Io=70)
1.90	75	1.92	80	220		
1.78	50				1.79	(200)TiAl-Si(I/Io=80)
1.63	30	1.68	40	204,311		
1.42	75	1.43	80	006,224		
1.34	60	1.36	60	400		
1.26	70	1.26	70	206,331		
1.16	70	1.17	80	117,422,333		
1.14	50	1.15	60	226,404		
1.10	45	1.08	40	008		

Table V presents a comparison of the measured I-spacings and intensities of a powder sample prepared from an Al rich Ti sample with $TiAl_3$ listed in the Powder Diffraction File.

No. 2-1121: $TiAl_3$ and verified by an arc melt prepared sample of $TiAl_3$.[38] It has been recently reported that a low-temperature superstructure of $TiAl_3$, tentatively designated Ti_8Al_{24} may result when the reaction temperature is below 640°C, and another similar phase Ti_9Al_{23} is also known.[32] The minute quantities of material available from this thin-film residue produced a powder pattern where all of the relatively weak lines were totally unobserved and the measurement accuracy was only slightly better than one percent. The absence of the weak lines prevented observation of the superstructure lines and the inaccuracy of the measurement prevented differentiation of the major strong lines of $TiAl_3$, Ti_8Al_{24} and Ti_9Al_{23}, all of which have reflections at diffraction angles which are within one percent of each other.

The $TiAl_3$ diffraction pattern has two relatively strong reflections at d=4.30A and d=3.51A which are absent in Ti_9Al_{23} and weak or absent in Ti_8Al_{24}. These lines are prominent in the diffraction pattern of the Al rich Ti residue. Therefore, this residue must be substantially composed of $TiAl_3$.

Four lines appeared in the diffraction pattern of the residue which are not identifiable within the context of the substances thus far described. A possible identification of one of these lines with the strong (111) reflection from Si is indicated. The other three lines may result from the Ti-Al-Si ternary which is found to result when the Si-Ti-Al system is heated for times substantially longer than necessary to consume all the Ti in $TiAl_3$. This interpretation is substantiated by the observation that the sample exhibiting these four lines was heat treated just to the point where all the Ti would have

been consumed based on the growth kinetics. X-ray diffractometer measurements of Ti-Al samples deposited on SiO_2 substrates which were heated sufficiently to form $TiAl_3$ did not exhibit the three lines described in the previous case. Orientation effects could mask the presence of these lines in the diffractometer pattern, however, so this result does not resolve the difficulty entirely.

Continued heating of the Si-Ti-Al system causes the three lines in question to strengthen and the $TiAl_3$ lines to disappear. Furthermore, electron microprobe analysis indicates that the Ti layer previously void of Si and rich in Al become Si rich as the heating progresses beyond the point where the entire Ti layer is converted to $TiAl_3$. The ratio of Si to Al is found to be approximately three to one after the latter phase develops. A powder pattern of the Si rich Ti phase is illustrated in the left column of table VI. This sample was heated to 500°C for 60 minutes. This heat treatment was considerably longer than necessary to consume the entire 1500Å layer of Ti deposited on this sample. The measured pattern is compared with the powder pattern of a Si rich Si-Al-Ti ternary identified in the Powder Diffraction Files as 18:71 ($Ti_7Al_5Si_{12}$).[37] The pattern measured from the Si rich Ti layer matches the referenced pattern except that three planes with large spacing are totally missing from the spectrum. The 2.02A and 1.22A lines measured in the powder sample may result from Al since other strong Al lines are present at 2.34Å and 1.43Å. This would suggest that the material might be Ti_2 (Al_1Si_3), which is reported to have a c axis dimension approximately ¼ the height of $Ti_7Al_5Si_{12}$.[37,39] The three to one compositional ratio of Si to

TABLE VI

PDF: 18-71

Si Rich Ti Layer		$Ti_7Al_5Si_{12}$			Other
D(A)	I/Io	D(A)	I/Io	(h k ℓ)	
		3.33	70	013	
		2.99	70	015	
		2.63	60	017	
2.34	90				Al (111) I/Io =100
2.26	50	2.26	70	0012	
2.21	100	2.21	100	116	
2.02	60	2.03	70	0111	or Al (200) I/Io =47
1.99	40				possibly β reflection from strong α-line at 2.21Å
1.79	70	1.79	80	200	
1.43	50				Al (220) I/Io =22, $TiAl_3$ I/Io =22
1.40	50	1.40	80	20$\underline{12}$	
1.29	40	1.29	70	11$\underline{18}$	
1.27	40	1.26	70	220	
1.22	70	1.22	70	0121	and/or Al(311) I/Io =24

Table VI presents a comparison of the measured d-spacing and intensities of a powder sample prepared from a Si rich Ti sample with $Ti_7Al_5Si_{12}$ listed in the Powder Diffraction File.

Al found from the electron microprobe results favors the identifaction of $Ti_2(Al_1Si_3)$. However, this would require the entire 1.22Å line measured in the powder pattern to result from Al. The relative intensities measured for the Al lines suggest that at least some of the intensity in the 1.22Å line does not result from Al. If this line at least in part results from the ternary then a cell of relative c axis dimension c/3 compared with $Ti_7Al_5Si_{12}$ would be consistant with the other data. This may suggest that the material is a somewhat modified ordering of either $Ti_7Al_5Si_{12}$ or $Ti_2(Al,Si)$ with a tetragonal cell of approximate dimensions a = 3.58Å and c = 9.04Å. More evidence would be required to substantiate this argument. The material will be tentatively identified as a modified form of $Ti_7Al_5Si_{12}$ at this time.

CHAPTER V

FAILURE MECHANISM IN Ti-Al CONTACTS TO Si

In this chapter a Ti-Al metallization system used to form electrical contacts to Si is described. The metallization system is found to have very desirable properties provided the post deposition heat treatment does not proceed beyond a certain critical time and temperature. If heated beyond the critical value the Ti-Al contact to Si is destroyed. The key to understanding and controlling this failure mechanism is found to be the rate kinetics of $TiAl_3$ formation described in chapter IV. Hence, this work provides a practical example of the use of backscattering to understand and control thin film metal systems used in the semiconductor industry. The model developed in this work may be useful in analyzing other thin film metal systems.

A brief description of properties of Al and Ti-Al contacts to Si is given to introduce the subject matter.

A. Al and Ti-Al Contacts to Si

Aluminum is perhaps the most widely used metal in Si integrated circuits. It forms excellent Ohmic contacts to heavily doped n- and p-type Si;[40] forms an excellent Schottky barrier on lightly doped n type material;[41] and has a low sheet resistivity compared with other metals which adhere well to Si and SiO_2.[42] Aluminum has two properties which are not desirable in metal contact applications to Si circuits. Electromigration is reported to be troublesome in high

current applications and Si pits in contact windows cause potential failures in shallow junction structures.[43,44]

A Ti-Al metallization scheme provides adequate electrical contact to heavily doped p and n type Si; adheres well to Si and SiO_2; and when suitably heat treated does not pit the Si in the contact holes.[21] In addition, it has been reported that electromigration is considerably reduced with a Ti-Al metal compared with Al.[45,46]

The electron microprobe and scanning electron and optical microscope are used in this work to investigate metallurgical properties of the Ti-Al system related to pits in the Si contact windows. Migration of Si into the Al layer is compared for Al and Ti-Al metallization. Silicon is found to migrate freely in the Al metal system in a manner consistent with reported results and the Si contacts are severely pitted.[42] No Si migration in the Al is found for the Ti-Al case and the Si contact area is unpitted provided the time and temperature of heat treatment does not proceed beyond a critical value. If heated beyond the critical point a deep pit forms in the Si contact area which generally renders it useless. The dramatic change in the contact from the unpitted case to the deeply pitted case is shown to be directly related to the consumption of the Ti layer in the formation of $TiAl_3$ and subsequent migration of Si from the contact areas into the surrounding regions where a Si rich Ti-Al-Si ternary forms. The unpitted contact is preserved in the Ti-Al contact to Si provided the entire Ti is not consumed in the formation of $TiAl_3$. Thus the rate of formation of $TiAl_3$ described in the previous chapter is the key to being able to design a Ti-Al system which will not be pitted during the post metallization heat treatments.

B. Results and Discussion

1. Silicon Dissolution into the Al Layer in Al-Ti and Al Metal Contacts

A schematic diagram of a cross section of an Al-Ti and Al metallization layer in the vicinity of a contact window is shown in figure 14. Contact windows generally range from 4 to 100 micrometers on a side in typical Si devices and integrated circuits. Several thousand Angstroms of SiO_2 are typically used to electrically isolate the metal layer from the semiconductor outside of the contact window. The Ti-Al system differs from the Al system in that a layer of Ti separates the Al from the Si and SiO_2 region.

The Ti-Al metalization can result in virtually unpitted Si contact areas after heat treatments which cause considerable pitting of the contact areas when Al metal is used. This can be directly seen from the scanning electron micrographs labelled A and B in figure 15. Contact patterned samples of both Ti-Al and Al metal layers were heated to 425°C for 30 minutes. The metal was subsequently etched from the surface and the substrates cleaved to reveal Si contact window areas. Micrograph A shows a contact window area from the sample which was covered with Ti-Al during the heat treatment. No Si erosion or pitting of the contact area can be seen in this case. In contrast, the contact area in micrograph B which resulted from a sample covered with Al during heat treatment shows substantial erosion in the Si contact area. The pits shown in this figure may result in shorts or unreliable behavior in shallow junction Si device structures. The pits in the Si contact have been shown to result from the diffusion of Si into the Al layer during heat treatment.[47] This

Fig. 14 A schematic representation of a cross sectional view of a Ti-Al and Al contact to Si is shown in this figure. In each case a Si-contact window formed by selectively removing the SiO_2 layer is shown.

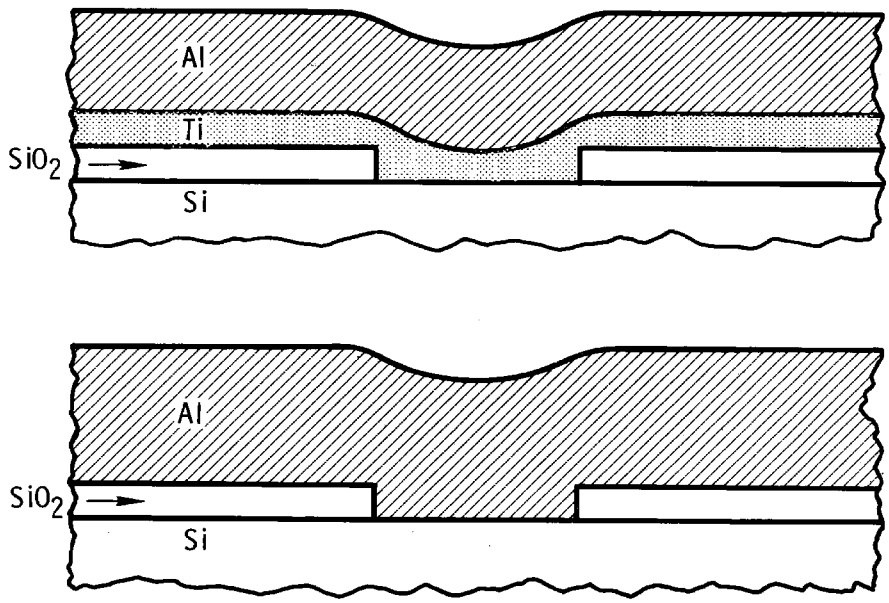

Figure 14

Fig. 15 This figure shows that a Ti prevents pit formation in Si contact windows. Samples with Ti-Al and Al metal deposited on contact patterned wafers were heated to 425°C for 30 minutes. The metal was then stripped from the surface and the samples cleaved and scanned to find a contact window intercepted by the cleavage plane. The upper (SEM) photo labeled A results from the Ti-Al system and no Si pits are seen, while (SEM) photo B seen in the lower portion of this figure results from the Al metal contacts and is heavily pitted.

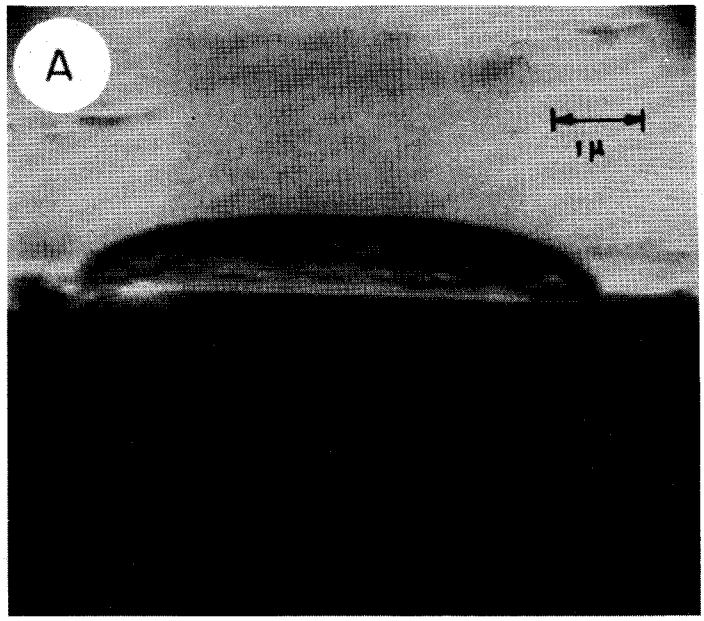

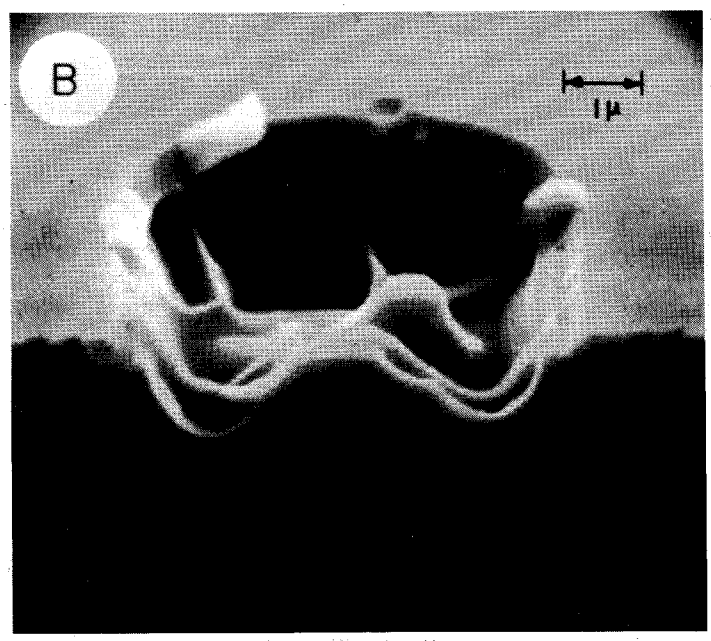

Figure 15

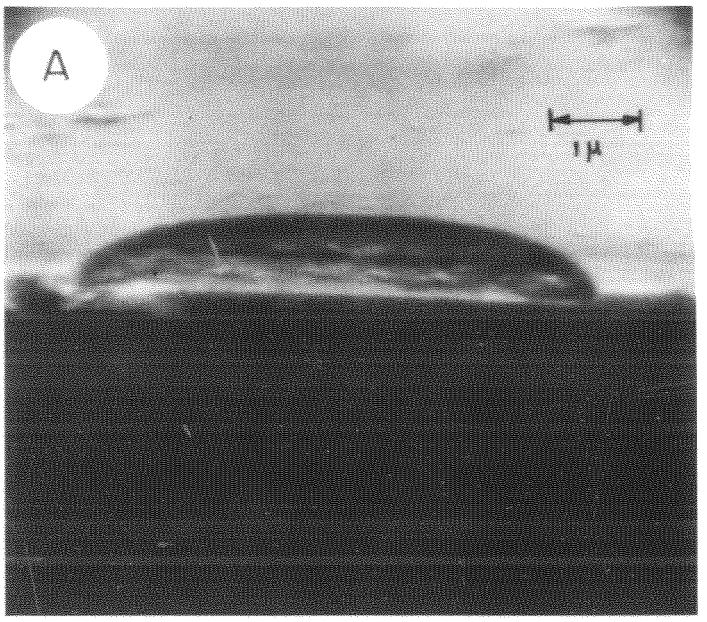

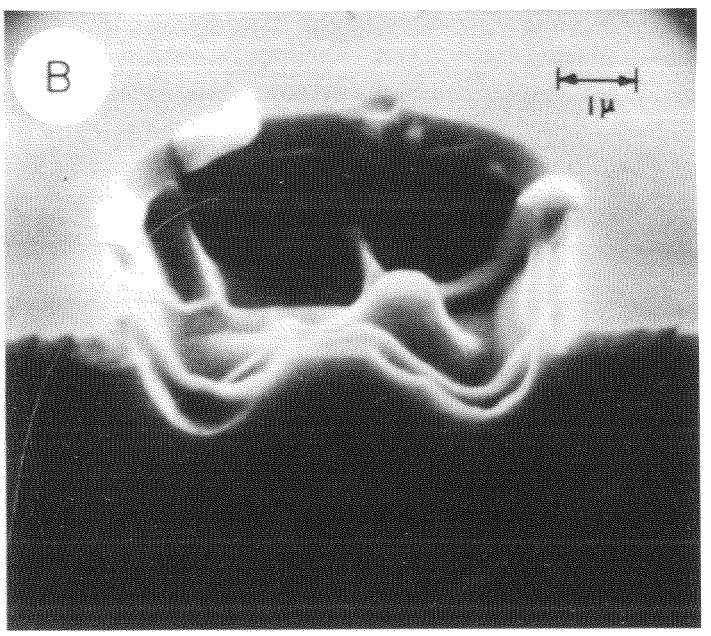

Figure 15

is substantiated in figure 16 which shows electron microprobe line scans of Ti-Al and Al metal layers in the vicinity of Si contact windows. In each case, the surface Al layer was illuminated with 5 kV electrons and the detector aligned for Si Kα x-rays. Both samples were heated to 400°C for 30 minutes prior to microprobe analysis. The TiAl sample shows no signs of Si diffusion into the Al layer, while in the Al case a definite Si signal is observed.

The results of the SEM and electron microprobe experiments shown in these two figures point out two important facts. First, Si dissolution into Al results in pits in the contact areas. Secondly, Ti acts as an effective Si diffusion barrier which prevents pits from forming in the Ti-Al metal contact system. This result makes the Ti-Al metal systems desirable for shallow junction device applications where Si pits potentially reduce yield and reliability.

The Si-Ti-Al system forms aluminide and silicide phases at relatively low temperatures, and the formation of these compound phases cause a drastic change in the Si contact windows which will be described in the following section.

2. Contact Failure in the Al-Ti Metalization System

The undesirable effects of the Al-Ti system manifest themselves dramatically in the sequence of SEM photos shown in Figure 17. The photo at the top of this figure was made in a similar manner to the ones shown in figure 15. The Al-Ti was heated to 500°C for 45 minutes, the metal stripped and the sample cleaved across a contact hole. In this case, a deep anisotropic hole appears in the Si contact window.[21] This hole is several microns deep and would certainly lead to a failure even with relatively deep underlying junction structures.

Fig. 16 This figure shows electron microprobe line scans of Ti-Al and Al metal layers in the vicinity of Si contact windows. The surface Al layer was illuminated with 5 KV electrons and scanned for Si Kα x-rays in each case. Both samples were heated for 30 minutes at 400°C prior to analysis. The Ti-Al case shows no Si in the Al while the Al case shows substantial Si migration.

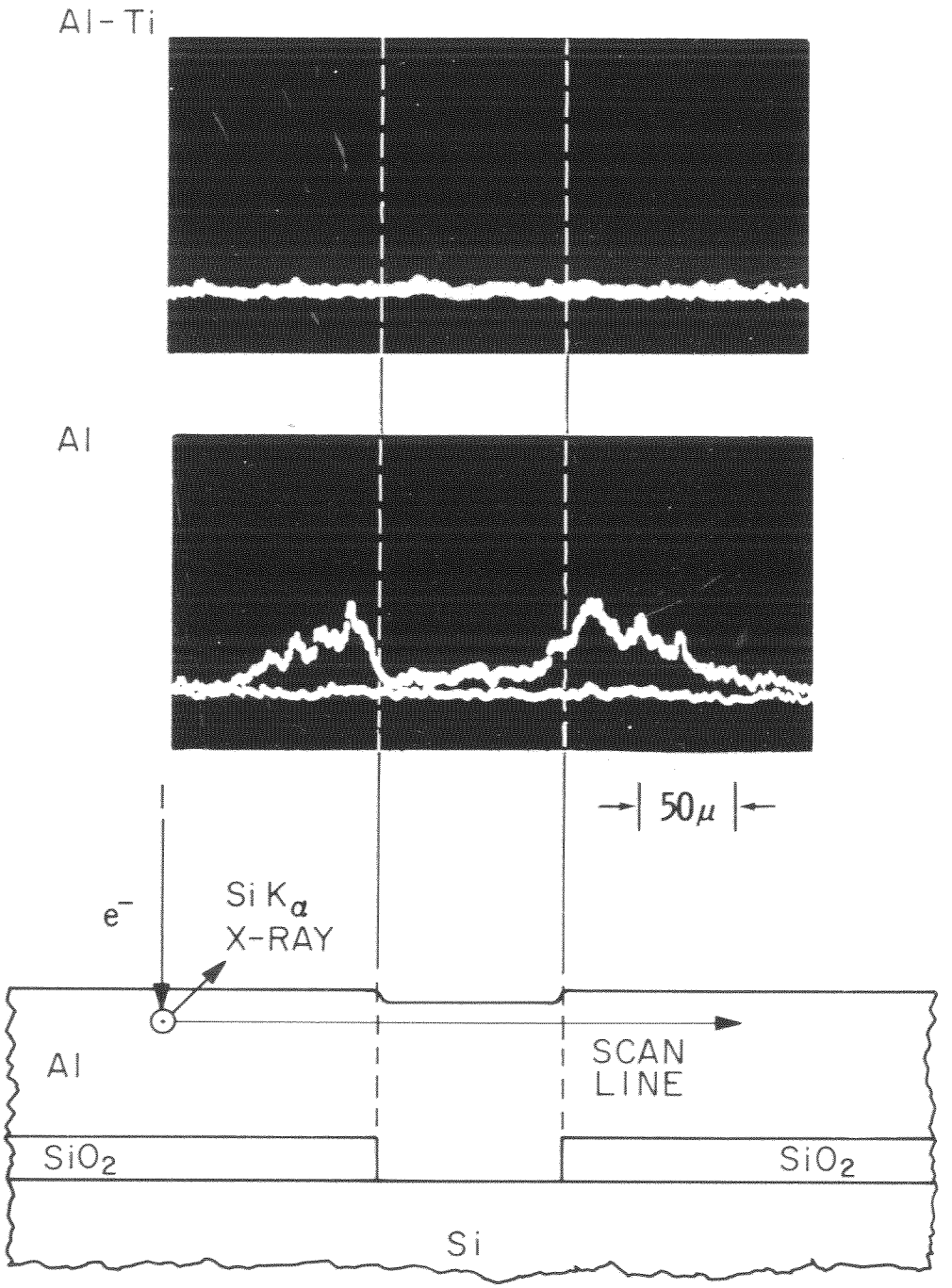

Figure 16

Fig. 17 The (SEM) micrographs shown in this figure illustrate the deep anisotropic holes which form in Si contact windows when the Ti-Al metal system is heated to 500°C. In the top photograph the sample was heated to 500°C for 45 minutes, stripped of metal and cleaved to reveal this deep hole which appears to preserve (111) Si planes in the contact area. The center photographs show a sample heated to 500°C for 15 minutes and cleaved in liquid nitrogen to preserve the shape of the Al metal. The bottom photograph shows a sample which was heated to 500°C for 45 minutes and stripped of Al only to reveal the remains of the Ti layer, which appears as a cap over the contact hole. The samples were all tilted 65° with respect to the electron beam axis.

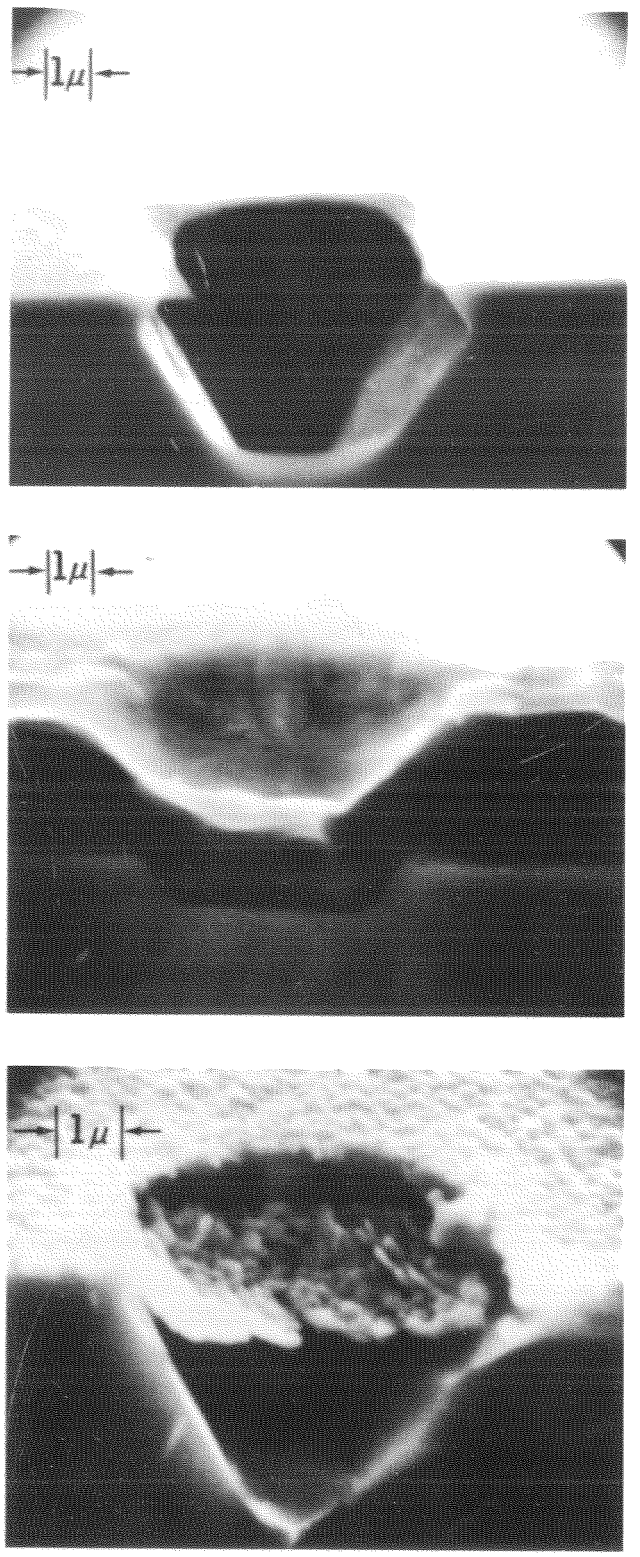

Figure 17

This is a drastic departure from the unpitted Ti-Al contact just described. If Ti-Al is to be used as a contact metal, the phenomenon leading to this deep pit must be avoided. The two accompanying photos in this figure provides a great deal of information about these Si pits. The center photo shows a contact region which was heated to 500°C for 15 minutes and cleaved in liquid nitrogen to retain the shape of the Al metal. The Si cleaved on a plane behind the contact hole, but the metal in the contact was retained. This photo indicates that Al displaced the Si originally in the contact region which corresponds to the Si pit in the upper photo. The lower photo shows that the Ti layer remains relatively intact during this process appearing as a cap over the contact hole. This sample was prepared by heating the Ti-Al contact to 500°C for 45 minutes, and then selectively removing Al metal only. It appears that some change occurred in the Ti layer which allows both Si and Al to migrate through it during the 500°C temperature treatment, while no migration of Si was evidenced during the 425°C heat treatment. A key to understanding this phenomena is found by noting that while the Ti layer is intact after the 500°C heat treatment its appearance is markedly different than before heat treatment indicating that it may have undergone a change of state.

3. Analysis of the Failure Mechanism in the Ti-Al Metal System

The deep pits in the Si contacts produced after the 500°C heat treatment of the Ti-Al system are directly related to compound phases which develop in the Si-Ti-Al system. In the previous chapter it was shown that when a thin film layer of Ti-Al is deposited on Si and heated between 400 and 500°C, a compound phase of $TiAl_3$ forms between

the Ti and Al layers.[19] It was also shown that after all the Ti was consumed in the $TiAl_3$ formation, a subsequent reaction produces a Si rich ternary Ti-Al-Si compound.

The next three figures will be used to show that these two compound phase formations are directly attributable to the pit formation.

The micrograph in figure 18 shows the visual appearance of the Ti layer in a Ti-Al contact which has been heated to 500°C for 45 minutes. The overlying Al layer was selectively etched to expose the Ti region. The Ti residue has a strikingly different appearance near the contact windows where the metal contact bare Si than away from them where a layer of SiO_2 approximately 3000Å thick separates the metal from the Si layer. A subsequent analysis indicated that Si pit formation begins just as the contrast develops in the Ti residue which differentiates the contact regions from the surrounding area. For a 600Å layer of Ti this corresponds to a temperature of 450°C for 30 minutes. Furthermore, the backscattering kinetics data from the last chapter indicate that approximately 600Å of Ti would be consumed in the $TiAl_3$ formation caused by this 450°C heat treatment. Hence, it appears that elimination of the Ti layer by formation of $TiAl_3$ leads to the dissolution of Si in the contact areas.

Chemical identifications of the visually contrasting regions in the Ti was made by means of the electron microprobe. This instrument was used to identify Si in the overlying Al layer and Al and Si in the Ti. The results of this identification can be seen in figure 19 where a sample heated to 475°C for 30 minutes is shown. The upper portion of this figure shows an electron microprobe topograph of the Si Kα x-ray emission from the Al layer. The lower portion shows a topograph of Si and Al abundance in the Ti residue. In this case, the overlying Al layer was

Fig. 18 This is a photomicrograph of a Ti-Al metal contact area which has been heated to 500°C for 45 minutes. The Al layer was then removed to reveal the Ti residue. The portion of the Ti layer near the contact window contrasts strongly with that far from the contact area.

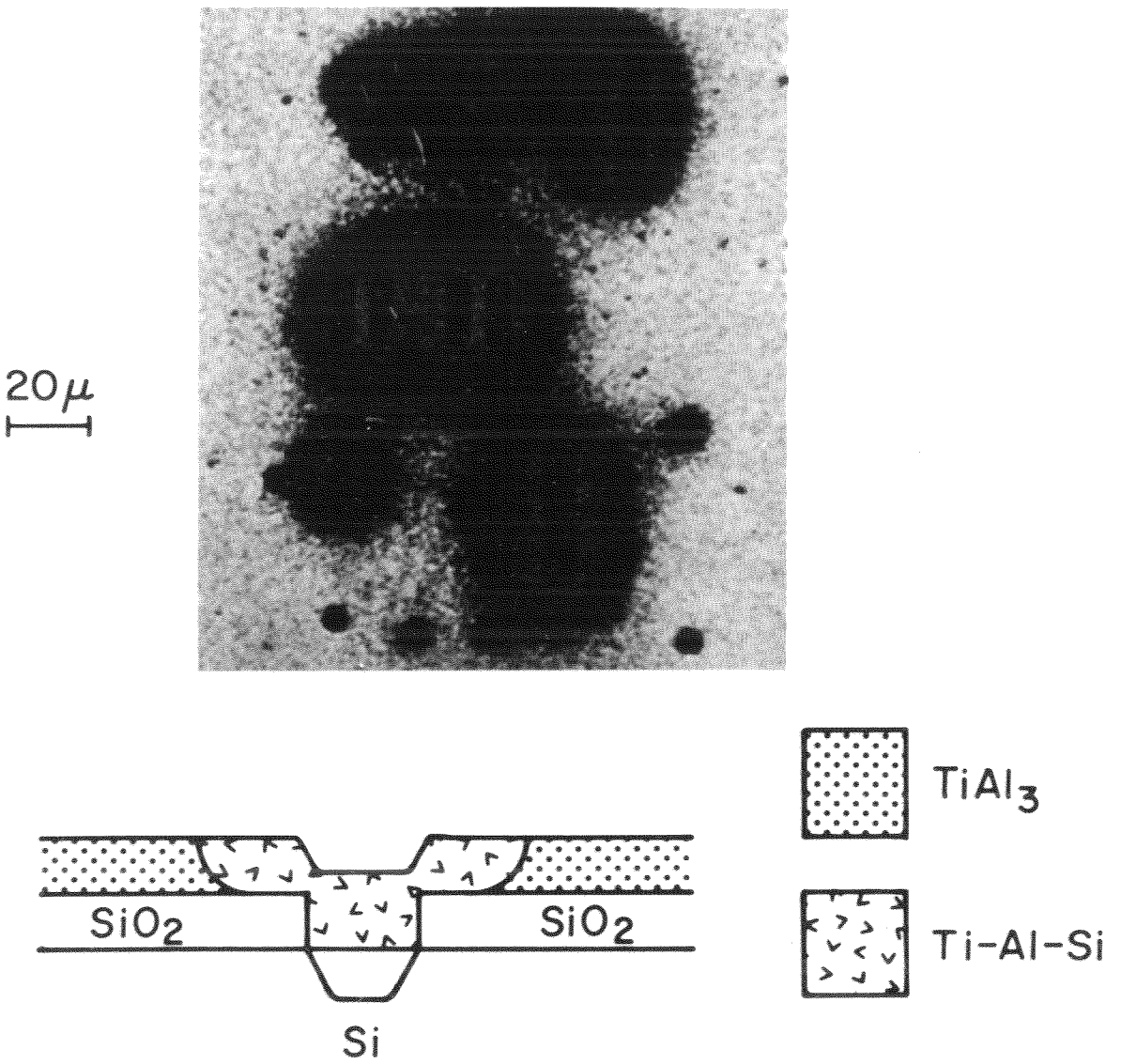

Figure 18

Fig. 19 This figure illustrates electron microprobe topographs of the Al and Ti residue regions of a Ti-Al metal contact which was heated to 475°C for 30 minutes. The upper topographs show the Si abundance in the Al layer, while the center and lower topographs reveal the Si and Al abundance respectively in the Ti residue. The Si rich region of the Ti layer appears to extend laterally approximately the same distance as the Si has migrated in the Al layer. The Si and Al rich Ti regions appear to be complementary.

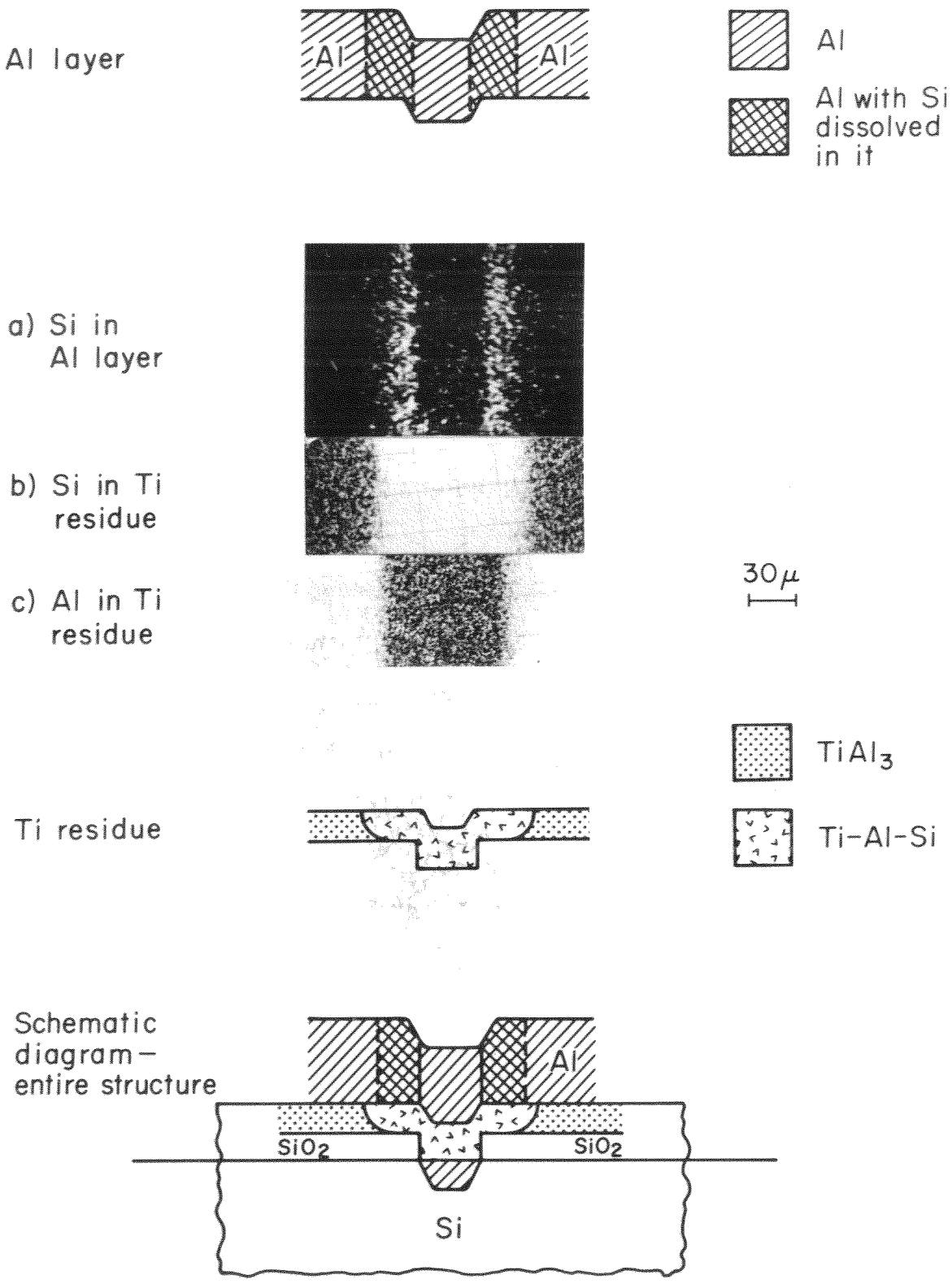
Al layer
Al
Al
Al
Al with Si dissolved in it
a) Si in Al layer
b) Si in Ti residue
c) Al in Ti residue
30μ
TiAl3
Ti-Al-Si
Ti residue
Schematic diagram – entire structure
Al
SiO2
SiO2
Si

Figure 19

selectively etched from the surface to allow direct analysis of the Ti residue with 5 kV electrons. These topographs show that in the vicinity of the contact window the Ti residue is Si rich, while far from the contact the residue is Al rich. It should also be noted that the Si and Al rich regions in the Ti layer do not overlap, and that the Si rich region in the Ti layer extends almost exactly the same distance outside of the contact area as the Si in the Al layer. This suggests that the Si rich region in the Ti is nourished by Si transported by the overlying Al. Corroborating evidence is shown in figure 20 where an electron microprobe is again used to display the abundance of Si dissolved in the Al layer near contact cuts for both Al and Al-Ti metalizations. In both cases the samples were heated to 500°C for 30 minutes. The Si has migrated substantially further in the case where no Ti layer is present. The effective diffusion coefficient of Si in Al would be reduced if a substantial flux of Si were diverted from the Al layer. Thus, it is reasonable to assume that the substantially shorter migration length of Si in the Al layer for the Al-Ti case results from a flux diversion of the Si into the Ti residue. Quantitative analysis of the Ti layer by the electron microprobe shows that in the Si rich region the abundance of Si is three times that of Al and that the total abundance of Si plus Al in this region is about equal to the Al abundance alone in the Al rich region. In the Al rich region of the Ti layer the Al abundance was found to be approximately three times that of Ti. This same ratio of Al to Ti was found in the Ti regions of large area Si-Ti-Al and SiO_2-Ti-Al samples which were heated and found in the last chapter to have the crystal structure of $TiAl_3$. Hence, it is reasonable that

Fig. 20 This figure illustrates that Si migrates further from a contact region in Al than for the Ti-Al case. This results from the diversion of the Si flux into the formation of the Si rich Ti-Al-Si ternary. The effect of this flux diversion is to reduce the effective diffusion length of Si in the layer. Both samples were heated to 500°C for 30 minutes.

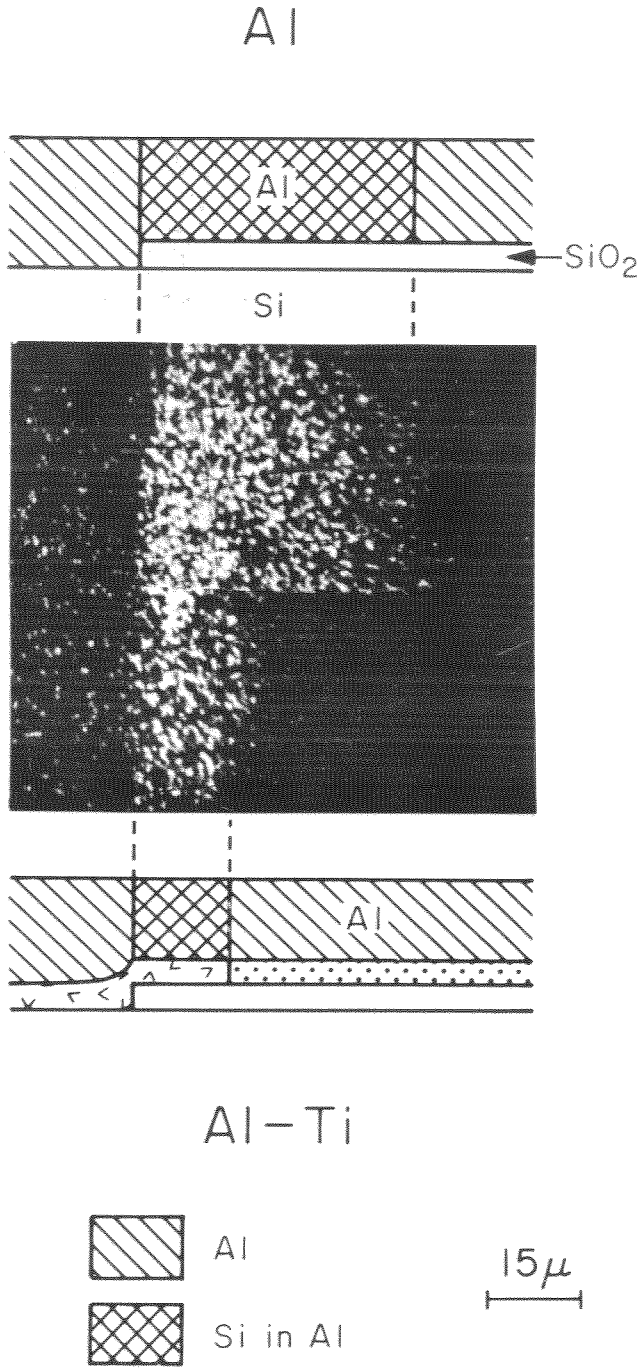

Figure 20

the Al rich Ti layer in the patterned wafers is composed of $TiAl_3$. Similarly, the Si rich portion of the Ti layer in these patterned samples were found to have approximately the same chemical composition as the Si rich Ti layers identified on large area samples in the last chapter as the crystallographic phase related to $Ti_7Al_5Si_{12}$.

It is reasonable to assume that the Si rich region of the Ti layer in these patterned samples is also composed of the Si rich Ti-Al-Si ternary. Finally, based on the data presented in the last three figures it is also reasonable that the Al layer provides the path needed to transport the Si laterally from the Si contact holes to the $TiAl_3$ layer which is then converted to the Si rich Ti-Al-Si ternary.

C. Summary of the Failure Mode in Ti-Al Contacts to Si

The Ti-Al contact failure process just described may be summarized in Fig. 21. This figure illustrates the effect of the $TiAl_3$ and Si rich Ti-Al-Si ternary formation in the vicinity of a contact hole. First the $TiAl_3$ formation begins across entire Ti layer. When all the Ti is consumed, Si begins to react with the $TiAl_3$ layer to produce the ternary phase. Silicon then migrates from the contact and diffuses into the Al layer while Al moves into area of removed silicon. The ternary layer then appears to extend beyond the contact window as the Si saturated Al provides Si to convert the $TiAl_3$.

The contact failure just summarized can be avoided by utilizing the relationship derived in Chapter IV to estimate the thickness of Ti consumed during heat treatment in the formation of $TiAl_3$. This

relationship states that the thickness of Ti consumed, X, in cm is related to the time of heat treatment, τ, in sec at a given temperature $X^2 = d\tau$, where $d \approx 0.15\ e^{-1.85/kT}\ cm^2/sec$. To avoid the contact failure the thickness of the deposited Ti layer must be greater than the thickness of Ti consumed during heat treatment.

Fig. 21 The basic contact structure is shown in (i). In (ii) $TiAl_3$ begins to form over the whole structure and in (iii) all the titanium has been consumed. At this point, the Ti-Si-Al ternary forms over the contact region (iv) and silicon begins migrating into the aluminum while aluminum displaces the migrating silicon in the contact hole. The majority of the silicon displaced from the contact hole is diverted into the $TiAl_3$ adjacent to the contact area to extend the ternary region.

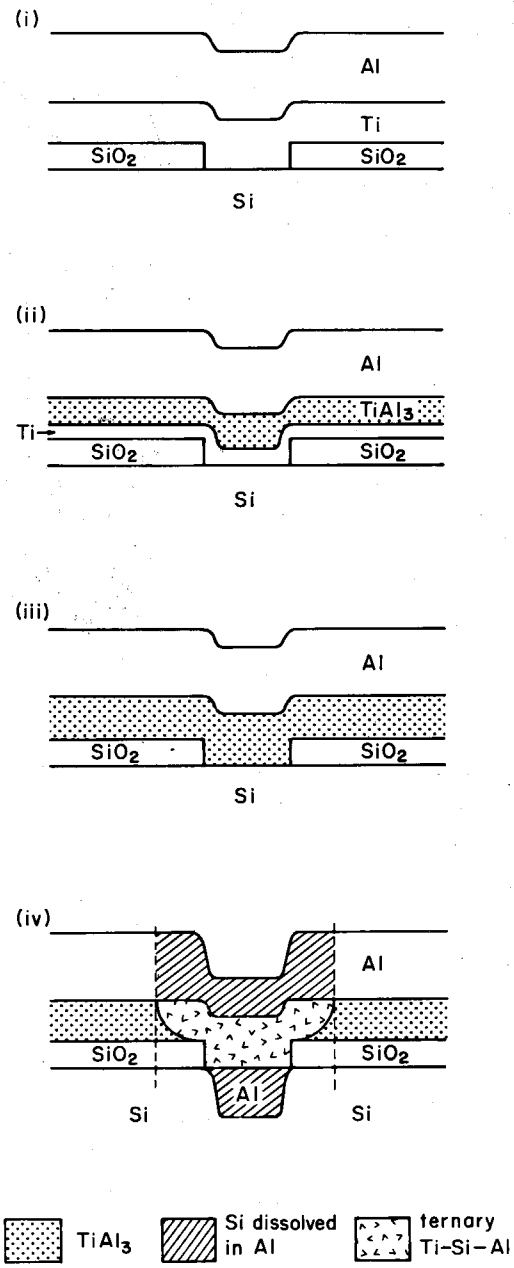
(i)
Al
Ti
SiO2
SiO2
Si
(ii)
Al
TiAl3
Ti
SiO2
SiO2
Si
(iii)
Al
SiO2
SiO2
Si
(iv)
Al
SiO2
SiO2
Al
Si
Si
TiAl3
Si dissolved in Al
ternary Ti-Si-Al

Figure 21

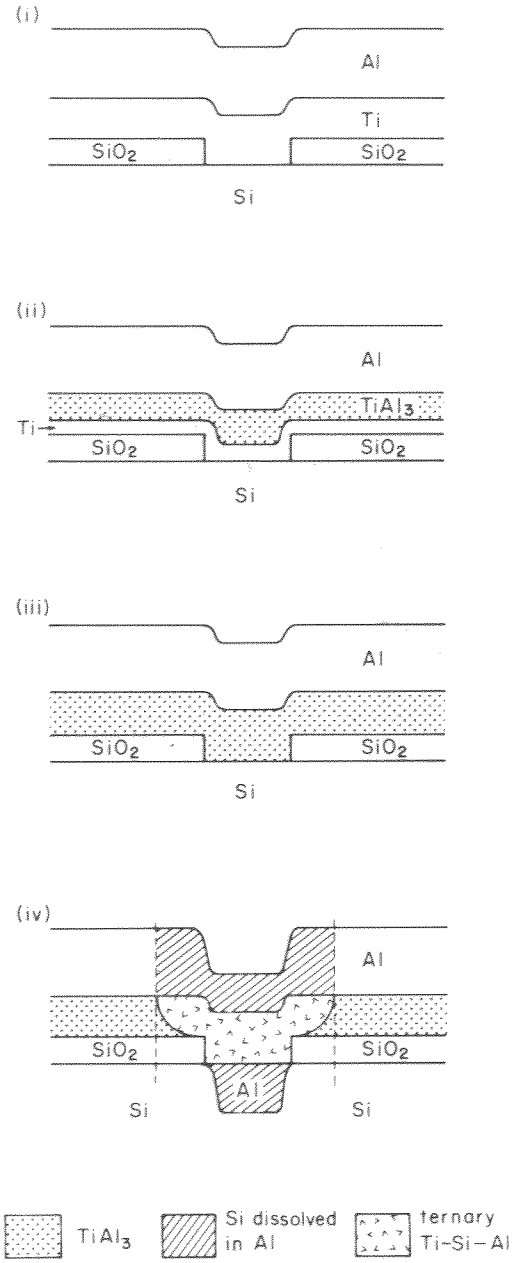
(i)
Al
Ti
SiO2
SiO2
Si
(ii)
Al
TiAl3
Ti
SiO2
SiO2
Si
(iii)
Al
SiO2
SiO2
Si
(iv)
Al
SiO2
SiO2
Al
Si
Si
TiAl3
Si dissolved in Al
ternary Ti-Si-Al

Figure 21

CHAPTER VI

SUMMARY

The backscattering analysis techniques developed in this work have provided a means of quantifying the rates of formation of compound phases in thin film structures. This information is of considerable importance since it has been found that metal-silicon and metal-metal systems form compound phases at relatively low temperatures.

The Pd-Si system provided an example where a uniform, highly oriented, single compound phase develops at very low temperatures. This system also illustrated the manner in which x-ray diffraction analysis may be used to complement backscattering to provide crystallographic identification and determine orientation effects of the compound phases which develop.

The backscattering technique demonstrated more of its power when applied to the double interface system of Si-Ti-Al. Backscattering analysis unambiguously showed that when this system is heated between 400 and 500°C a reaction occurs at the Ti-Al interface where a phase of composition $TiAl_3$ develops, while no reaction occurs at the Si-Ti interface. This information provides the key to understanding the complex interactions which occur when this system is heat treated. X-ray diffraction analysis again proved useful to identify the crystal structure of the compound phases which develop in this system. Both $TiAl_3$ and the Si rich ternary were identified by x-ray techniques,

although the electron microprobe was used in the identification of the ternary phase.

The usefulness of knowing the reaction products and growth kinetics of compound phases in thin film structures was illustrated in the study of the failure mechanism in the Ti-Al contact system to Si. This metallization scheme is used in the semiconductor industry, where it generally provides electrical contacts to Si with excellent characteristics.

A failure mechanism in this contact scheme, which occurs during heat treatment, was found to be directly related to the formation of $TiAl_3$ and the Si-rich ternary in the Si-Ti-Al system. The scanning electron microscope and electron microprobe were the essential tools used to study the structural properties of the Ti-Al contacts before and after failure. The chemical and visual characteristics of the Ti layer then provided the evidence necessary to relate the contact failure to the $TiAl_3$ and Ti-Al-Si ternary formation.

The consumption of Ti in the $TiAl_3$ formation proved to initiate the failure in this contact system. Once the Ti was eliminated in the $TiAl_3$ formation, the Si was free to diffuse from the contact areas. The formation of the Ti-Al-Si ternary provided a sink for the migrating Si which caused the contact areas to be destroyed.

The rate of consumption of the Ti layer in the formation of $TiAl_3$ was determined in the backscattering analysis. Knowledge of this rate allows the Ti layer to be chosen thick enough to avoid contact failure during heat treatment. Hence, the failure mechanism in this contact system can be avoided by design. The techniques developed

to analyze the failures in this metal contact system should be useful in analyzing and predicting failure mechanisms in other similar thin film metal systems.

APPENDIX

A. Backscattering Analysis

1. Backscattering Energy Loss Parameter

In a multilayer structure studied by backscattering the energy loss parameter [S] will change abruptly at the interface between the layers. In the following analysis a two-layer structure will be considered and the coordinates characterizing the two-layer system are given in Fig. (1A). The specific energy loss per unit length $\frac{dE}{dx}$ (eV/Å), which is a function of energy E, will be denoted S(E) and is related to the atomic stopping cross section ε(eV x cm^2/atom) through the expression

$$S(E) = \varepsilon(E)\ N \tag{1}$$

where N is the density (atoms/cm^3). The energy of the ^4He particles reaching the detector after scattering from atoms in medium I at depth t from the surface ($t < t_I$) is given by the specific energy loss in medium I, $S_I(E)$, kinematic factor k_M, and scattering angle θ ($\theta = 180° - \theta'$) as

$$E_I = k_M\left(E_o - \int_0^t S_I(E)d\ell_1\right) - \int_{-t/\cos\theta'}^{0} S_I(E,t)d\ell_2 \tag{2}$$

where it is specifically noted that $S_I(E)$ on the outgoing trajectory is a function of the depth, t, at which the backscattering collision occurred. Similarly for particles scattered at depth t in medium II ($t > t_I$) one obtains the following expression

Fig. 1A This figure shows the coordinates used for backscattering analysis of a layer of medium I on a substrate of medium II. The projectiles with energy E_o enter perpendicular to the substrate surface and are after scattering monitored in an angle θ'. For the mathematical treatment the line ℓ_1 is considered to have its positive direction into the sample and ℓ_2 its positive direction out from the sample. The origins of coordinates ℓ_1 and ℓ_2 are located at the sample surface.

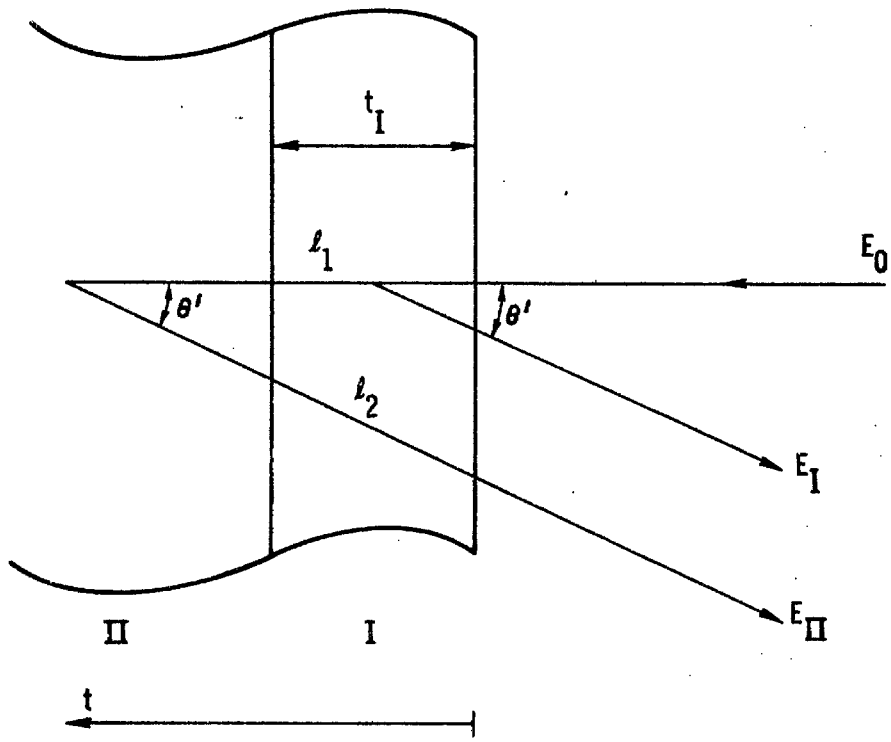

Figure 1A

$$E_{II} = k_M E_o - \int_0^{t_I} S_I(E)\,d\ell_1 - \int_{t_I}^{t} S_{II}(E)\,d\ell_1 - \int_{-t/\cos\theta'}^{-t_I/\cos\theta'} S_{II}(E,t)\,d\ell_2 - \int_{-t_I/\cos\theta'}^{0} S_I(E,t)\,d\ell_2 \tag{3}$$

where the dependence of both S_I and S_{II} on t is explicitly noted.

The differential form of the backscattering energy loss parameter [S] is defined as the negative derivative of the energy of the detected particles with respect to the position, t, of the backscattering event with a species of mass M. Differentiating (2) and (3) one obtains

$$[S]_M^I(t) = -\frac{dE_I}{dt} = K_M S_I(E_-(t)) + \frac{S_I(E_+(t))}{\cos\theta'} + \int_{-t/\cos\theta'}^{0} \frac{\partial}{\partial t} S_I(E,t)\,d\ell_2$$

$$\approx K_M S_I(E_-(t)) + \frac{1}{\cos\theta'} S_I(E_+(t)) \tag{4}$$

$$[S]_M^{II}(t) = -\frac{dE_{II}}{dt} = K_M S_{II}(E_-(t)) + \frac{S_{II}(E_+(t))}{\cos\theta'} + \int_{-t/\cos\theta'}^{-t_1/\cos\theta'} \frac{\partial}{\partial t} S_{II}(E,t)\,d\ell_2 + \int_{-t_1/\cos\theta}^{0} \frac{\partial}{\partial t} S_I(E,t)\,d\ell_2 \tag{5}$$

$$\approx K_M S_{II}(E_-(t)) + \frac{1}{\cos\theta'} S_{II}(E_+(t))$$

where $E_-(t)$ is the energy of the projectile just prior to collision and $E_+(t)$ is the energy just after collision. While these expressions are mathematically correct, the terms involving the integrals of $\frac{\partial}{\partial t} S$ are generally small and therefore ignored in evaluating [S].

If the specific energy loss factors are treated as constants over the range of integration of (2) and (3), these expressions may be

explicitly integrated to yield

$$E_I = K_M E_o - \left[K_M S_I(\bar{E}_{in\ I}) + \frac{1}{\cos\theta'} S_I(\bar{E}_{out\ I})\right] t \qquad (2)'$$

$$E_{II} = K_M E_o - \left[K_M S_I(\bar{E}_{in\ I}) + \frac{1}{\cos\theta'} S_I(\bar{E}_{out\ I})\right] t_I$$

$$- \left[K_M S_{II}(\bar{E}_{in\ II}) + \frac{1}{\cos\theta'} S_{II}(\bar{E}_{out\ II})\right] (t-t_I) \qquad (3)'$$

where $\bar{E}_{in\ I}$ and $\bar{E}_{in\ II}$ are the average energies of the projectiles on the incoming path in regions I and II and $\bar{E}_{out\ I}$ and $\bar{E}_{out\ II}$ are the average energies in these regions on the outgoing path. The bracketed expressions in (2)' and (3)' have the functional form of the approximate expressions for [S](t) given in (4) and (5). Thus the terminology $[S]_M^I = K_M S_I(\bar{E}_{in\ I}) + \frac{1}{\cos\theta'} S_I(\bar{E}_{out\ I})$ and $[S]_M^{II} = K_M S_{II}(\bar{E}_{in\ II}) + \frac{1}{\cos\theta'} S_{II}(\bar{E}_{out\ II})$ is introduced to simplify expressions (2)' and (3)' to

$$E_I = K_M E_o - [S]_M^I \cdot t \qquad (2)''$$

$$E_{II} = K_M E_o - [S]_M^I \cdot t_I - [S]_M^{II} \cdot (t - t_I) \qquad (3)''$$

These expressions define the linear approximation of (2) and (3) which allow the energy loss to be considered a depth scale. This linear approximation is accurate to within 5% for Pd_2Si and $TiAl_3$ films less than 5000Å in thickness.

2. Backscattering Yield

The yield H (counts per channel) of the backscattering energy spectrum from a material with density N (atoms/cm^3) is given by

$$H = Q(\delta\Omega)\left(\frac{d\sigma}{d\Omega}\right)(N\Delta t) = Q(\delta\Omega)\left(\frac{d\sigma}{d\Omega}\right)\left(N\,\frac{(\Delta E)_{ch}}{[S]}\right) \qquad (6)$$

where Q is the number of incoming particles, $\delta\Omega$ is the solid angle subtended by the detector, $\frac{d\sigma}{d\Omega}$ is the scattering cross section, and $\Delta t = (\Delta E)_{ch}/[S]$ is the depth interval in the material corresponding to the width of one energy channel $(\Delta E)_{ch}$ of the multichannel analyzer. From relation (6) it is clear that abrupt changes in composition usually result in an abrupt change in the backscattering yield H.

3. Composition

The principles outlined above form the basis for extracting composition as a function of depth in compounds from backscattering spectra. For palladium-silicide discussed in the present work there are clearly resolved regions in the backscattering spectrum corresponding to Si and Pd respectively. The ratio of the heights of the plateaus in the spectrum, H_{Si} and H_{Pd}, using relation (6), gives the ratio of the densities N_{Si} and N_{Pd} as a function of energy E and hence depth t,

through the following expression:

$$\frac{N_{Pd}}{N_{Si}} = \frac{H_{Pd}}{H_{Si}} \times \frac{[S]_{Pd}^{Pd_2Si}}{[S]_{Si}^{Pd_2Si}} \times \frac{\left(\frac{d\sigma}{d\Omega}\right)_{Si}}{\left(\frac{d\sigma}{d\Omega}\right)_{Pd}} \qquad (7)$$

To calculate N_{Pd}/N_{Si} the specific values of [S] and $\left(\frac{d\sigma}{d\Omega}\right)$ are not required but rather the ratios $[S]_{Pd}^{Pd_2Si}/[S]_{Si}^{Pd_2Si}$ and $\left(\frac{d\sigma}{d\Omega}\right)_{Si} \Big/ \left(\frac{d\sigma}{d\Omega}\right)_{Pd}$ where it should be noted that $[S]_{Pd}^{Pd_2Si}$ and $[S]_{Si}^{Pd_2Si}$ are evaluated for specific energy loss per unit length, S, for the compound using Bragg's rule,[27] i.e., $S_{Pd_2Si} = (2\varepsilon_{Pd} + 1\varepsilon_{Si})N_{Pd_2Si}$.

The ratio $[S]_{Pd}^{Pd_2Si}/[S]_{Si}^{Pd_2Si}$ in principle can now be calculated from known values of stopping powers $S(E)$ for Pd and Si. Such a calculation, using the additivity of stopping powers in a compound entails the knowledge of the unknown ratio of N_{Pd}/N_{Si}. However, because of the monotonic behavior of the stopping power function $S(E)_{Pd_2Si}$ it is possible to bracket the ratio $[S]_{Pd}^{Pd_2Si}/[S]_{Si}^{Pd_2Si}$ between .98 and 1.12, which corresponds to the extreme cases pure Pd and pure Si respectively. Thus the ratio for any compound of Pd and Si must fall in this narrow interval and any value within the range may be used in an iterative procedure to converge to the actual composition ratio of the compound.

In a situation where the composition is relatively constant in depth and the energy width of the layer can be estimated from the backscattering spectrum, the ratio $[S]_{Pd}^{Pd_2Si}/[S]_{Si}^{Pd_2Si}$ can be conveniently estimated in the following manner. As explained in the section on backscattering analysis the width of each component in the spectrum is proportional to the parameter [S], i.e., $\Delta E_{Si} = t[S]_{Si}^{Pd_2Si}$ and $\Delta E_{Pd} = t[S]_{Pd}^{Pd_2Si}$ where t is the thickness of the compound. Thus

$[S]_{Pd}/[S]_{Si}$ is directly given as the ratio of the energy widths $\Delta E_{Pd}/\Delta E_{Si}$. The laboratory cross sections $\left(\frac{d\sigma}{d\Omega}\right)_{Si}(E)$ and $\left(\frac{d\sigma}{d\Omega}\right)_{Pd}(E)$ are given by the Rutherford formula

$$\left(\frac{d\sigma}{d\Omega}\right) = \left(\frac{Z_1 Z_2 e^2}{2E \sin^2\theta}\right)^2 \frac{\left[\cos\theta + \sqrt{1 - \left(\frac{m_1}{m_2}\sin\theta\right)^2}\right]^2}{\sqrt{1 - \left(\frac{m_1}{m_2}\sin\theta\right)^2}} \tag{8}$$

where θ is the laboratory angle, E is the laboratory energy, Z_1 and m_1 are the atomic number and mass of the ^{4}He projectile and Z_2 and m_2 are the corresponding values for the target materials Si or Pd. The ratio $\frac{d\sigma}{d\Omega}_{Si} \Big/ \frac{d\sigma}{d\Omega}_{Pd}$ does not vary with energy.

A somewhat different approach is applicable in the case of uniform composition with depth. The ratio of the densities of Pd and Si may be estimated in the following manner. The total number of counts A_{Pd} and A_{Si} in the backscattering spectrum from each element in the compound are defined as

$$A = \int \frac{H}{(\Delta E)_{ch}}\, dE \tag{9}$$

From Eq. (6) one derives

$$\int \frac{H}{(\Delta E)_{ch}}\, dE = \int Q\,(\delta\Omega)\left(\frac{d\sigma}{d\Omega}\right) N\, dt \tag{10}$$

where the interval of integration is the silicide region. N may then be removed from the integral leading to the following expression:

$$A = Q(\delta\Omega)N\int\left(\frac{d\sigma}{d\Omega}\right)[E(t)]dt \tag{11}$$

from which the ration N_{Pd}/N_{Si} is derived as

$$\frac{N_{Pd}}{N_{Si}} = \frac{A_{Pd}}{A_{Si}} \times \frac{\int\left(\frac{d\sigma}{d\Omega}\right)_{Si} dt}{\int\left(\frac{d\sigma}{d\Omega}\right)_{Pd} dt} \tag{12}$$

From the expression (8) of the cross section it is clear that $\left(\frac{d\sigma}{d\Omega}\right)_{Pd}(E) = c \times \left(\frac{d\sigma}{d\Omega}\right)_{Si}(E)$ where c is a constant independent of energy. From this expression the ratio of the integrals in Eq. (12) is

$$\frac{\int\left(\frac{d\sigma}{d\Omega}\right)_{Si} dt}{\int\left(\frac{d\sigma}{d\Omega}\right)_{Pd} dt} = \frac{1}{c} \quad \frac{\int\left(\frac{d\sigma}{d\Omega}\right)_{Si} dt}{\int\left(\frac{d\sigma}{d\Omega}\right)_{Si} dt} = \frac{1}{c} \tag{13}$$

Hence, the final expression becomes

$$\frac{N_{Pd}}{N_{Si}} = \frac{A_{Pd}}{A_{Si}} \times \frac{\left(\frac{d\sigma}{d\Omega}\right)_{Si}}{\left(\frac{d\sigma}{d\Omega}\right)_{Pd}} \tag{14}$$

where the ratio of the integrals over the cross sections is independent of energy.

B. Channeling Measurements

When an ion beam is incident parallel to a major crystallographic direction in a single crystal, there is a drastic reduction in the number of backscattered particles as compared to the situation when the beam is incident in a random direction (not aligned with a major axis). For example, a ~ 30 fold reduction in scattering yield is observed when

the 2-MeV $^4He^+$ beam used in this study is aligned with a <111> direction in a Si single crystal.[25] This effect is sensitive to the degree of perfection of the crystalline substrate. For example, heteroepitaxial layers of Si on spinel have been studied by the channeling technique. The distribution in depth of lattice imperfections was extracted from channeling spectra.[48] The crystal orientation of solid-phase grown Ge layers on Ge has been studied by the channeling effect.[49] The Ge layers were found to be epitaxial. In this study channeling was used to study the orientation of the Pd_2Si film with respect to the underlying Si substrate.

Figure (2A) shows aligned and random backscattering spectra from a Pd_2Si film formed on a <111> Si substrate. The sample was annealed at 400°C for 30 minutes which allowed all of the evaporated Pd to form Pd_2Si. To orient the <111> direction of the Si substrate with respect to the beam, channeling techniques were used on a portion of the sample on which the Si surface was exposed. The beam was then translated, maintaining the alignment, to a portion of the sample covered by Pd_2Si and the energy spectra were recorded. In both the part of the energy spectrum corresponding to scattering from Pd in Pd_2Si and the part corresponding to scattering from Si in Pd_2Si there is a ~25% reduction of the aligned yield as compared to the random yield. Also for scattering from Si in the substrate under the Pd_2Si there is a ~15% reduction of the aligned yield as compared to the random yield. This reduction in aligned yield is small compared to what is seen on uncovered Si and is due

Fig. 2A Random and aligned energy spectra for 2 MeV ^{4}He scattering from a Pd_2Si film formed on a <111> Si substrate. The sample initially consisted of 3000Å Pd and was heat treated at 400°C for 30 minutes.

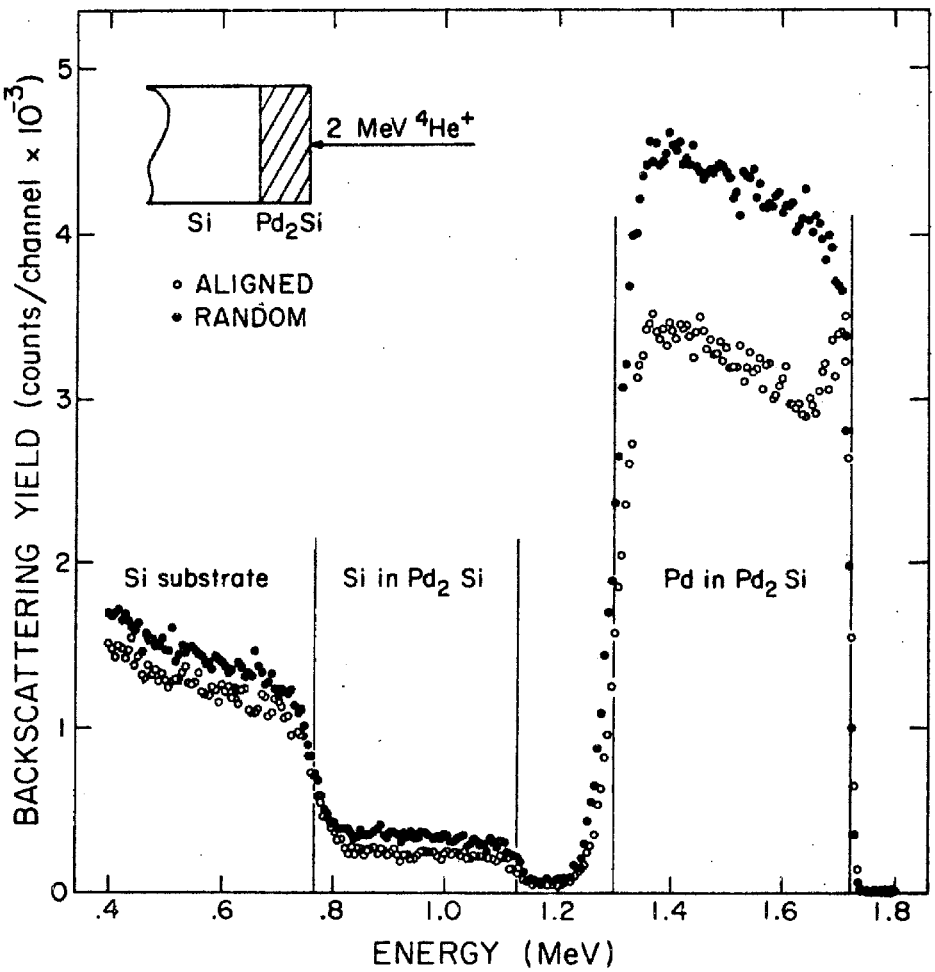
2 MeV $^4He^+$
Si
Pd_2Si
ALIGNED
RANDOM
Si substrate
Si in Pd_2 Si
Pd in Pd_2 Si
BACKSCATTERING YIELD (counts/channel x 10^{-3})
ENERGY (MeV)
0
1
2
3
4
5
.4
.6
.8
1.0
1.2
1.4
1.6
1.8

Figure 2A

to multiple scattering of the ^4He ions in the overlying Pd_2Si layer.[23]

Similar measurements were done on films formed on <110> and <100> Si substrates. There was no evidence of a reduction of the aligned yield in these cases. Therefore, the channeling behavior in the <111> case was investigated in more detail. The degree of preferred orientation of the Pd_2Si layers formed on <111> substrates was found to be strongly influenced by the temperature of formation. Samples heat treated between 275°C and 650°C were analyzed by 2-MeV ^4He ion channeling. The minimum yields ranged from 80% for the lowest temperature to 20% for the highest.

More insight can be obtained if the scattering yield is measured as a function of the angle between the beam and the crystallographic axis of interest. Figure 3A shows an angular scan for scattering from Pd and Si in a Pd_2Si film formed on a <111> Si substrate. The midpoint of the curves corresponds to incidence parallel with the <111> direction in the Si substrate. The channeling dips are usually characterized by the half width measured at half minimum of the dip, $\Psi_{1/2}$, and by the normalized minimum yield for perfect alignment. As discussed in Chapter III, it was found that the <00.1> direction of Pd_2Si was preferentially aligned perpendicular to the substrate surface. Therefore, the observed effects are attributable to channeling in the <00.1> direction of Pd_2Si. In this direction of Pd_2Si there are separate Pd and Si atomic rows. In earlier investigations on channeling in diatomic lattices it has been found that for moderate depth into the crystal (< 5000Å) channeling from the two kinds of atomic rows can be considered

Fig. 3A Angular variation of the normalized scattering yield from Pd and Si in a Pd_2Si layer formed on a <111> substrate by heating at 400°C for 30 minutes.

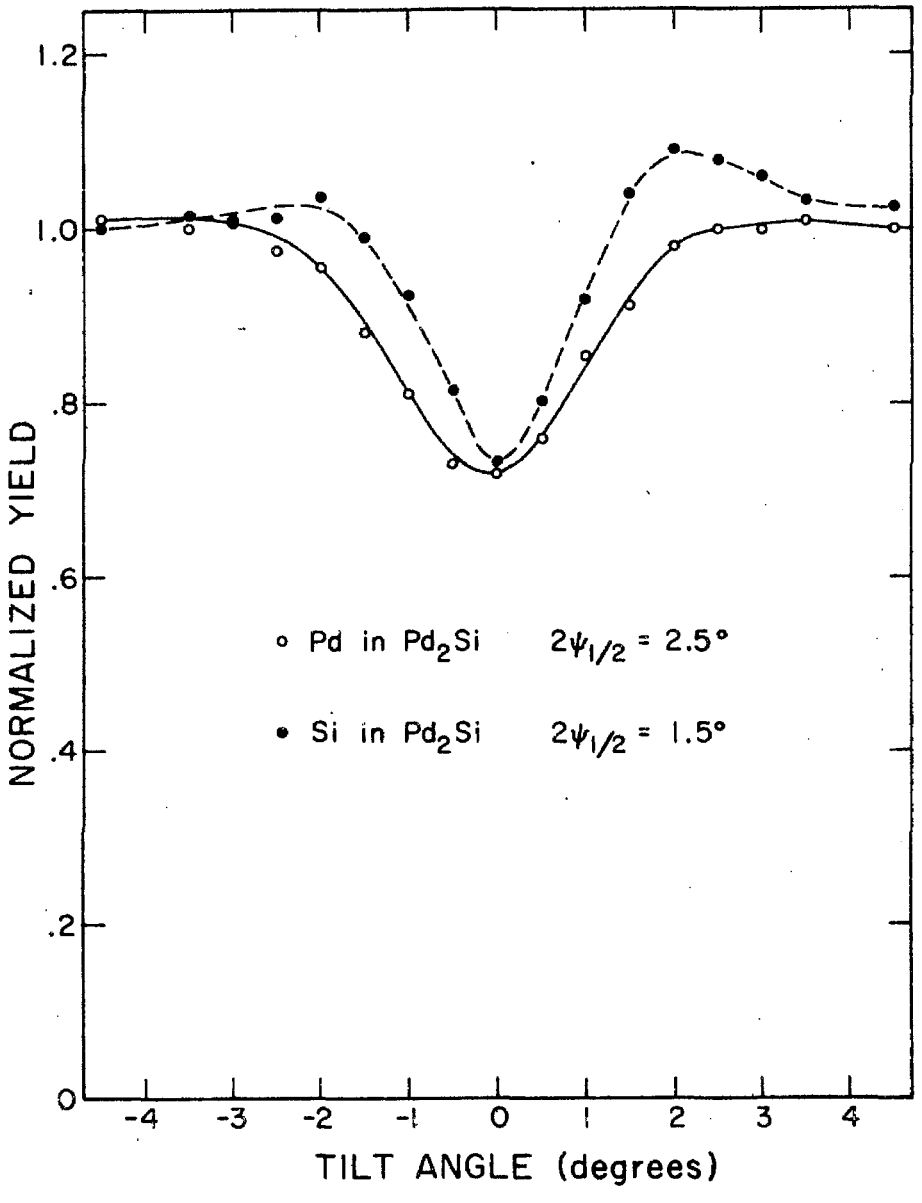
1.2
1.0
.8
.6
.4
.2
0
NORMALIZED YIELD
-4
-3
-2
-1
0
1
2
3
4
TILT ANGLE (degrees)
o Pd in Pd2Si 2ψ1/2 = 2.5°
• Si in Pd2Si 2ψ1/2 = 1.5°

Figure 3A

separately and the half widths can be estimated using the continuum theory for channeling.[50] The half width $\Psi_{1/2}$ is by this theory given as $C \times \Psi_1$, where C is a constant depending on the thermal vibrations of the lattice atoms and Ψ_1 is the characteristic angle for channeling.[25] The constant C is usually close to unity. The angle Ψ_1 is .62° and 1.1° for scattering from Si and Pd rows respectively and the ratio is .55. The corresponding measured values of $\Psi_{1/2}$ are .75° and 1.25°. The ratio of the measured half widths .6 is roughly in agreement with the calculated ratio which indicates that the steering of the ^4He ions is done by separated Si and Pd atomic rows.

As was remarked earlier, the minimum yield from the uncovered Si substrate is ~ 3%. Thus, the measured minimum yield values for the Pd_2Si film are substantially higher than from a perfect single crystal, and fall between what is expected from a single crystal and that of a random structure. This finding can be interpreted in two ways: (1) roughly 25% of the Pd_2Si film is perfectly epitaxial and the rest is not aligned with the substrate, (2) the Pd_2Si film is almost epitaxial i.e., there is a small spread in the alignment of the <00.1> axis of the Pd_2Si. For example, if this spread is of the order of the characteristic angle for channeling, simple estimates give a minimum yield of 60% from the channeling data.[51] The half width of the channeling distribution increases as the energy is decreased allowing a greater fraction of the Pd_2Si film to fulfill the channeling condition. Several Pd_2Si films formed on <111> Si substrates showed such a behavior. From this it is concluded that the Pd_2Si layers are almost epitaxial with a spread in orientation of the order of 1 degree. This

interpretation is consistent with the X-ray data presented in Chapter III.

REFERENCES

1. A. J. Khambata, Introduction to Integrated Semiconductor Circuits, New York, John Wiley and Sons, Inc. (1963).

2. T. Kawamura, D. Shinoda and H. Muta, Appl. Phys. Lett. 11, 101 (1967).

3. R. A. Tolla and R. P. Sopher, IBM J. Res. Dev. 13, 226 (1969).

4. J. M. Anderson and M. P. Lepselter, Solid-State Elec. 13, 1011 (1970).

5. W. V. T. Rush and C. A. Burrus, Solid-State Elec. 11, 1011 (1970).

6. C. J. Kircher, Solid-State Elec. 14, 507 (1971).

7. W. D. Buckley and S. C. Moss, Solid-StateElec. 15, 1331 (1972).

8. A. Shepela, Solid-State Elec. 10, 477 (1973).

9. H. J. Goldschmidt, "Interstitial Alloys," Plenum Press (1967).

10. M. Hansen and K. Anderko, Constitution of Binary Alloys," McGraw-Hill (1958).

11. J. S. Kirkaldy, Can. J. Phys. 36, 917 (1958).

12. P. Duwez, trans. A S M 60, 607 (1967).

13. I. V. Mitchell, M. Kamoshida and J. W. Mayer, J. Appl. Phys. 42, 4378 (1971).

14. A. Hiraki, M. A. Nicolet, and J. W. Mayer, Appl. Phys. Lett. 18, 178 (1971).

15. R. W. Bower and J. W. Mayer, Appl. Phys. Lett. 20, 359 (1972).

16. J. M. Caywood, private communications.

17. C. J. Kircher, J. W. Mayer, K. N. Tu and J. F. Ziegler, Appl. Phys. Lett. 22, 81 (1973).

18. R. W. Bower, J. W. Mayer, D. Sigurd, unpublished data.

19. R. W. Bower, "Low Temperature Intermetallic Phase Formation on Evaporated Ti and Al Layers on Si," Submitted J. Appl. Phys.

20. H. Muta and D. Shinoda, J. Appl. Phys. 43, 2913 (1972).

21. R. W. Bower, Appl. Phys. Lett. (In Press). "Characteristics of Al-Ti Contacts on Si."

22. R. W. Bower, submitted Solid-State Elec. "Failure Mechanism in Ti-Al Contacts to Si."

23. E. Rimini, E. Lugujjo and J. W. Mayer, Phys. Rev. B6, 718 (1972).

24. C. S. Barrett and T. B. Massalski, Structure of Metals, McGraw-Hill (1966).

25. J. W. Mayer, L. Eriksson and J. A. Davies, Implantation in Semiconductors, Academic Press (1970).

26. R. W. Finne and D. L. Klein, J. Electrochem. Soc. 114, 965 (1967).

27. W. H. Bragg and R. Kleeman, Phil. Mag. 10, 318 (1905).

28. J. M. Caywood, Acta. Met. (in press).

29. L. Frank, Phys. Stat. Sol. (a) 15, 251 (1973).

30. K. Anderko' and K. Schubert, Z. Metallk. 44, 307 (1953).

31. A. Nylund, Acta Chem. Scand. 20, 2381 (1966).

32. F. J. J. van Loo and G. D. Rieck, Acta Metallurgica, 21, 61 (1973).

33. M. A. Nicolet, J. W. Mayer and I. V. Mitchell, Science 177, 841 (1972).

34. G. Brauer, Z. Inorg. Chem. 4, 242 (1939).

35. P. Duwez and J. L. Taylor, J. Metals 4, 70 (1952).

36. E. Ence and H. Margolin, J. Metals 9, 484 (1957).

37. A. Raman and K. Schubert, Z. Metallk. 56, 44 (1965).

38. Arc melt sample prepared by P. Duwez for comparison of powder diffraction lines with thin film compound.

39. O. Schob, H. Nowotny and F. Benesovsky, Planseeber. Pulv. Metal. 10, 65 (1962).

40. R. C. Hooper, J. A. Cunningham, J. G. Harper, Solid-State Elec. 8, 831 (1965).

41. A. Y. C. Yu and C. A. Mead, Solid-State Elec. 13, 97 (1970).

42. L. E. Terry and R. Wilson, Proc. IEEE, 57, 1580 (1969).

43. J. R. Black, IEEE Trans. EO-16, 338 (1969).

44. R. J. Anstead and S. R. Floyd, EO-16, 381 (1969).

45. R. J. Patterson, J. Electrochem. Soc. 119, 238C (1972).

46. J. C. Andersson, Thin Solid Films, 12 1 (1972).

47. J. O. McCaldin and H. Sankur, Appl. Phys. Lett. 19, 524 (1971).

48. S. T. Picraux, J. Appl. Phys. 44, 587 (1973).

49. V. Marrello, J. M. Caywood, J. W. Mayer and M. A. Nicolet, Phys. Stat. Sol. (a) 13, 531 (1972).

50. R. Hellborg, Physica Scripta 3, 279 (1971).

51. D. Sigurd, R. W. Bower and W. F. Van der Weg, California Institute of Technology, unpublished work.